DUCTILITY AND CHEMICAL REACTIONS AT THE INTERFACE BETWEEN NICKEL AND MAGNESIUM OXIDE SINGLE CRYSTALS

by

DIDERICUS PETRUS HERMANNUS HASSELMAN

A THESIS SUBMITTED IN PARTIAL FULFILMENT OF
THE REQUIREMENTS FOR THE DEGREE OF
MASTER OF APPLIED SCIENCE

in the Department
of
MINING AND METALLURGY

We accept this thesis as conforming to the standard required from candidates for the degree of MASTER OF APPLIED SCIENCE.

_____

_____

Members of the Department of
Mining and Metallurgy

THE UNIVERSITY OF BRITISH COLUMBIA
August 1959

In presenting this thesis in partial fulfilme the requirements for an advanced degree at the University of British Columbia, I agree that the Library shall make it freely available for reference and study. I further agree that permission for extensive copying of this thesis for scholarly purposes may be granted by the Head of my Department or by his representatives. It is understood that copying or publication of this thesis for financial gain shall not be allowed without my written permission.

Department of Mining and Metallurgy

The University of British Columbia,
Vancouver 8, Canada.

Date December 11, 1959

ABSTRACT

An investigation was conducted on the interaction between nickel metal and single crystals of magnesium oxide. The nickel was cleaned with purified hydrogen gas at 800°C and melted under vacuum (5×10^{-5} mm. Hg) in contact with the magnesium oxide. The interface was examined metallographically. The formation of compounds at the interface was examined by X-ray diffraction techniques.

The magnesium oxide was plastically deformed by thermal stresses which occurred on cooling. Slip occurred on four slip planes only. The slip sources were present in the surface at a depth not exceeding ten microns. They were in the form of dislocation half-loops introduced in the surface during cleavage. The introduction of these half-loops was due to the formation of cleavage steps. Rows of dislocation half-loops were due to the multiplication of a half-loop on a slip plane oriented in the direction of propagation of the cleavage crack.

Bond formation consisted of the formation of a magnesium-nickel compound (Mg_2Ni). The bond strength exceeded the stress for brittle fracture of magnesium oxide. Attack of the magnesium oxide occurred preferentially at the perimeter of the interface. This led to groove-formation, which resulted in a large hysteresis of wetting.

The diffusion of nickel into magnesium oxide seemed to take place mainly by diffusion along dislocations.

ACKNOWLEDGEMENT

The author is indebted to Mr. W.M. Armstrong for his supervision and encouragement and to Mr. R. Butters for his technical advice and assistance. The author is also especially indebted to Dr. E. Teghtsoonian and Mr. K.G. Davis for many helpful discussions.

The work was financed by Research Grant 7510-32 provided by the Defence Research Board of Canada.

SUMMARY OF STAFF COMMENTS AT THESIS PRESENTATION

December 9, 1959.

The staff was in general agreement that this was a very acceptable thesis. Considerable ingenuity in both experimental technique and in interpretation of results has been demonstrated by the candidate. Furthermore, he has proven his ability to design and execute good experiments and assess the results with a minimum of supervision. His oral presentation and defence of his thesis were both of good quality.

Some dissatisfaction was expressed concerning the validity of the X-ray evidence offered to substantiate the presence of Mg_2Ni compound at the interface between MgO and Ni drop. The candidate did not appear to understand the complete basis for the identification, based on both d spacings and relative line intensities. Accordingly, it is very doubtful that his interpretation of the X-ray films is correct. Similar objections apply to the identification of the NiO. It should be noted that this does not affect the major part of the thesis in any way.

It was also suggested that some of the conclusions concerning the dislocation mechanisms operative during the cleavage and deformation processes were only barely warranted by the experimental evidence put forward.

Additional minor corrections were as follows:

page 63, paragraph 2:

"During evaporation of the drop the term $\gamma_{Ni} \cos \theta$ continuously decreases."

This should read:

"During evaporation of the drop the component of the $\gamma_{Ni} \cos \theta$ term parallel to plane surface in the direction of γMgO decreases."

In addition, it is felt that the interpretation in terms of the groove formation and the ensuing modification through the angle β is not as significant as the candidate suggests.

page 93, last line: ". . . which contained little or no nickel."

should be: ". . . . which contained little or no metallic nickel."

W. M. Armstrong,
Professor of Metallurgy.

TABLE OF CONTENTS

Table of Contents (cont'd.) Page

Table of Contents (cont'd.) Page

FIGURES

Figures (cont'd.)

Figures (cont'd.)

TABLES

DUCTILITY AND CHEMICAL REACTIONS AT THE INTERFACE BETWEEN NICKEL AND MAGNESIUM OXIDE SINGLE CRYSTALS.

I. INTRODUCTION

A. General Purpose and Scope

Recently attempts have been made to combine the properties of metals and ceramics to produce a material suitable for use at high temperatures. At these temperatures, metals often fail as materials of construction through low strength, low creep resistance or poor resistance to oxidation or other attack. In contrast, ceramics at these temperatures have in general good strength, creep resistance and oxidation resistance but as compared with metals they are brittle. If we could combine these properties of metals and ceramics, the material produced would have very desirable properties for high temperature application.

In the development of these materials the major emphasis thus far has been on the development of useful materials on a mainly empirical basis. The art of preparing the materials, commonly referred to as 'cermets', is far in advance of a scientific understanding of the fundamental factors involved. These factors[1-8] include metal-ceramic reactions, surface and interfacial energies and constituent properties such as strength, ductility, oxidation resistance and thermal conductivity. In this paper the author reports on further investigations of the reactions between metal and ceramics.

Physical wetting of the ceramic by the metal is a major factor in producing an effective bond. This can be studied by considering the

interfacial energy involved. A low interfacial energy is equivalent to strong bonding, although other factors, such as interfacial stresses arising as cooling, affect the bond resulting at room temperature. For metals and ceramics of interest, little is known of the individual surface energies, much less of the interfacial energies and factors affecting them. At high temperatures the sessile-drop method[9,10,11] can be employed very effectively for measurements of this type. The angle of contact or wetting angle is then an indication of wettability of the ceramic by the metal.

The important reactions between the metal and ceramic are the formation of chemical compounds at or near the interface. Modifications of the materials present at the interface change the bonding forces. The chemical reactions which modify the interface depend on the thermodynamics of the system. The amount of these reactions depend on the atmosphere as well as on the composition. Unfortunately thermodynamic data is usually incomplete and a study of interfacial compounds must often be accomplished by experimental methods only.

Strong bonding between metal and ceramic can also be affected by the ability of the metal to diffuse into the ceramic.[8,12] This way a strong bond develops between the metal and the metal-enriched ceramic.

The properties of interest in cermet bodies include strength and creep resistance at elevated temperatures, corrosion and oxidation resistance, thermal expansion and thermal shock resistance. The individual components and composition employed have a considerable effect on these properties. Many properties, however, cannot be evaluated on the basis of the properties of the constituents.

Strength and creep at elevated temperatures are affected by the

refractoriness of the metal component employed. It is therefore expected that such composition as thoria-tungsten[13] are expected to maintain their strengths at elevated temperatures, even though their room temperature strength may be less than other compositions. The fact that the strengths of cermet bodies may be higher[2] than the component strengths has not been completely explained.

Corrosion and oxidation resistance of cermets depends on the resistance of the components and on the nature of the products formed. Oxidation resistance generally is due to the formation of an oxidation layer which prevents further oxidation.

One of the major limitations of ceramic materials for many applications is their poor thermal-shock resistance as compared with metals. Thermal-shock resistance increases with high thermal conductivity, high tensile strength, low coefficient of expansion and low modulus of elasticity. If, however, the ceramic concerned possessed a certain degree of ductility so that it would deform plastically,the cermet produced would be fairly resistant to thermal shock. In addition, if the metal and ceramic would have coefficients of thermal expansion which are reasonably well matched, the stresses caused by differences in expansion of the components would be low enough such that brittle fracture can not occur. A survey of the available metals and ceramics show that a combination of magnesium oxide and nickel may have some of the desirable properties as discussed above. Magnesium oxide has a high melting point,[14] is chemically stable and it has been shown that single crystals exhibit considerable ductility.[15-19] Nickel has a reasonably high melting point (1455°C); it has good resistance to chemical attack and its coefficient of expansion almost identical with the coefficient of expansion of magnesium oxide.[20,21] Consequently, these materials were chosen for a study of the interactions

between metals and ceramics.

B. Previous Work.

Nickel-magnesia interactions were intensively investigated by McFarlane, Jr.,[22] also by Kingery.[4] It was found by melting a nickel pellet on a polycrystalline magnesia block that the adherence of nickel to magnesia was excellent. The wetting angle was approximately 110°, while between the nickel and magnesia a sharp interface was found to exist. McFarlane[22] noticed a black discoloration around the magnesia, which confirms the result obtained by Economos and Kingery[3] who obtained a black coloration with nickel and magnesia although in their case it concentrated itself around the grain boundary.

The high bond strength between magnesia and nickel could not be explained satisfactorily. The possibility of the formation of a compound such as nickel oxide or the formation of a solid solution such as nickel oxide-magnesium oxide were investigated by X-ray analysis but no evidence for the existence of a compound or solid solution could be detected. It was felt that the presence of nickel oxide could be responsible for the bond between magnesium oxide and nickel. Magnesium oxide and nickel oxide form a continuous range of solid solutions[23] as shown in Fig. 1. The bond would then exist of a layer of nickel oxide adhering to the magnesium oxide and the nickel adhering to the nickel oxide. However, the amount of nickel oxide present may be too small to be detected by X-ray analysis.

Investigations[24,25] of the interaction between metal vapours and single crystals of magnesium oxide have shown that the magnesium oxide is not attacked by lithium, sodium, potassium and calcium. Copper, however, etched the surface of the crystals of magnesium oxide. The reactions between polycrystalline magnesium oxide and refractory metals such as molybdenum, silicon,

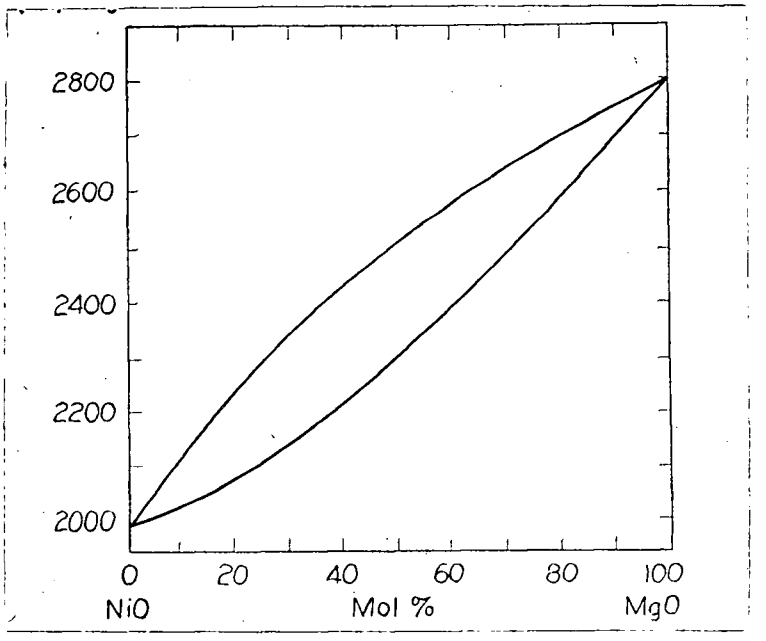

Fig. 1. MgO-NiO binary system.

titanium and zirconium showed that the metal penetrated the magnesium oxide along the grain boundaries and in all cases but molybdenum, reacted with the magnesium oxide by either forming an interfacial layer or by corroding the surface of the magnesium oxide.

The diffusion of metals into single crystals of magnesium oxide was investigated by Turnbull.[26] It was found that ruthenium, copper and barium do not diffuse interstitially. Iron, nickel and cobalt, however, do diffuse and the diffusion coefficients were determined.

The mechanical properties of magnesium oxide are currently being investigated.[15-19] It was observed that single crystals of magnesium oxide exhibit considerable ductility and it was felt that this could lead to the development of a ductile ceramic.[15] To determine the plastic properties, the single crystals of magnesium oxide were subjected to tension, bending and compression. It was observed[27] that magnesium oxide is most ductile when under compression and least when under tension. This is attributed to

the fact that under tension it is easier for crack formation to occur which then leads to brittle fracture. Johnston, Stokes and Li[19] investigated the fracture mechanism and found the ductility to be a function of the plastic deformation already present explained by the fact that regions of plastic flow act as barriers to the propagation of cracks. Investigations of the temperature dependence of the ductility showed that the magnesium oxide can be deformed to a much greater extent[27] before brittle fracture occurs at high temperatures (1500°C) than at low temperatures.

The effect of surface condition on the ductile properties was investigated by Stokes, Johnston and Li,[18] who introduced slip sources in the magnesium oxide by sprinkling the surface with 46-mesh carborundum particles. It was observed that slip occurred at a lower stress level in sprinkled crystals than in unsprinkled crystals. Atmospheric conditions did not seem to affect the plastic properties as had been observed[28] in materials of the same crystal structure such as potassium chloride. Other observations, however, seem to contradict this.

The mechanical properties of nickel-magnesia cermets were investigated by McFarlane, Jr.[22] He found that partly oxidized specimens were generally stronger than unoxidized ones. Most significant was that thermal shock did not lead to fracture. It was also found that the transverse strength of specimens subjected to series of thermal shock had increased rather than decreased.

C. Specific Aims of the Present Investigation.

The initial purpose of this investigation was to study the interaction between nickel metal and single crystals of magnesium oxide in order to be able to draw conclusions about the bonding mechanisms between metals and

ceramics in general. From the work done on the nickel-magnesium oxide system it could be concluded that little was known of the interactions between nickel and magnesium oxide. The specific aim of the present investigation was to study the interactions by all possible techniques such as X-ray analysis of reaction products at the interface, metallographic examination of perpendicular and tapered sections through the interface and X-ray fluorescence to study the diffusion of the nickel into the magnesium oxide. In addition, measurements of the wettability of the magnesium oxide by the liquid nickel were planned.

II. EXPERIMENTAL

A. Materials.

1. Magnesium oxide.

The single crystals of magnesium oxide used throughout the investigation were transparent. High Purity Optical Grade Magnesium Oxide supplied by Norton Company. This material is available in large irregular pieces with dimensions approximately 3x2x2 cms. such as shown in Fig. 6. Table I shows a typical chemical analysis. Qualitative analysis by means of X-ray fluorescence. showed a trace of iron only.

TABLE I

Material	Percentage
% SiO_2	less than .20
% Fe_2O_3	less than .15
% CaO	less than .20
% Al_2O_3	less than .35
% MgO	balance

Examination with polarized light revealed[17] the occasional occurrence of internal stresses. The seemed to be localized and were thought to be due to the existence of inclusions.

The crystal structure of magnesium oxide is the rocksalt-structure and is based on two interpenetrating face-centered cubic lattices, the lattice sites of the one lattice occupied by magnesium ions and the lattice sites of the other lattice occupied by oxygen ions. Because of its crystal structure it possesses perfect cleavage usually along {100} planes and occasionally along

{111} planes. In this investigation use was made of this property in the preparation of thin platelets on top of which the nickel could then be melted in order to study its interaction with the magnesium oxide (see Fig. 6). A typical (100) cleavage face is shown in Fig. 2. The lines running diagonally across the picture are so-called 'cleavage steps'[29] and are produced when cleavage is started on more than one cleavage plane and by the intersection of screw dislocations and suitable subgrain boundaries by the cleavage crack. Their height ranges from a few Angstroms to approximately 0.1 micron.

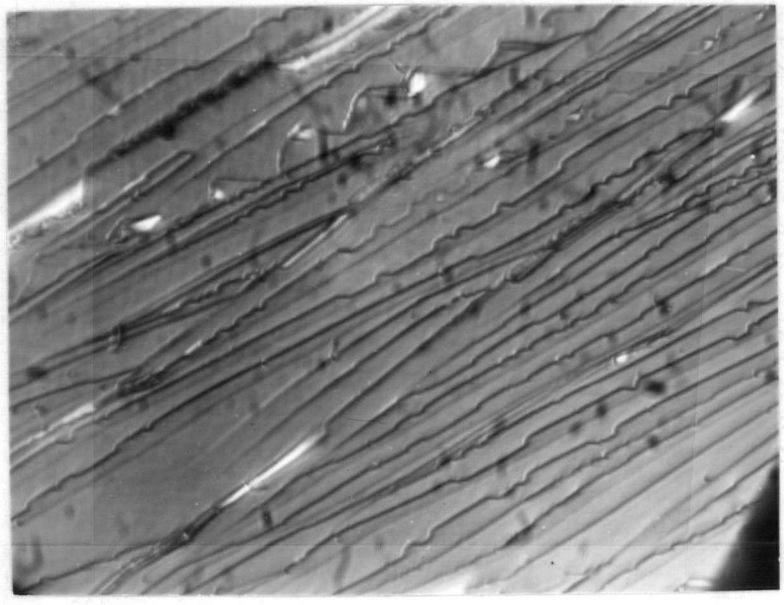

Fig. 2. Typical (100) cleavage face of magnesium oxide (x100).

Nickel

The nickel used in this investigation was supplied by Sherritt Gordon Mines Ltd. and Mond Nickel Co. Ltd., and was in the form of powder, and in the case of Sherritt Ni No. C525 also in the form of rolled strip, approximately .05 cm. thick. The chemical analyses of the various nickels are

given in Table II.

TABLE II

Analyses of Nickel Materials

Material	Analysis (maximum percent)					
	Ni	Co	Cu	Fe	S	C
Sherritt Ni No. C525	Bal.	.08	0.029	0.022	0.016	0.01
Sherritt high purity Ni	Bal.	.008	0.009	.004	.006	.08
Sherritt high Sulphur Ni	Bal.	.061	.013	.011	.020	.011
Mond carbonyl Ni	Bal.	.005	.008	0.007	.002	0.091

B. Apparatus

The apparatus was designed with the following objectives:

1. to produce temperatures as high as 1800°C by induction heating and vacuums as high as 5×10^{-5} mm. of Hg.

2. to permit the introduction of reducing atmospheres at pressures less than atmospheric pressure and

3. to allow measurements of drops at temperatures greater than the melting points of the alloys used.

The equipment is shown in Figs. 3 and 4.

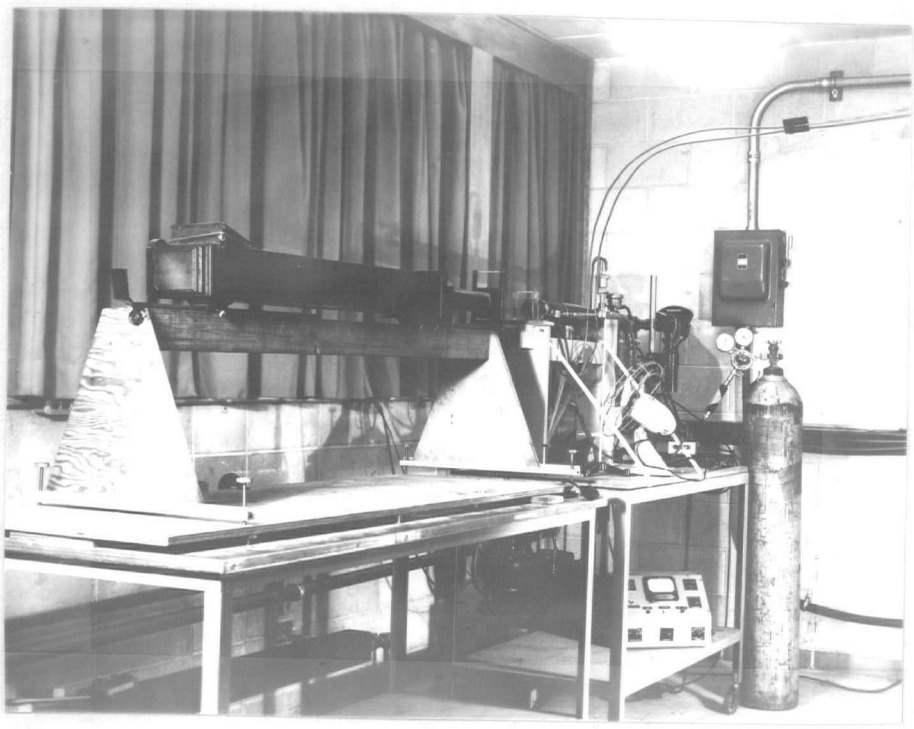

Fig. 3. The apparatus assembly of the induction furnace vacuum system and optical system

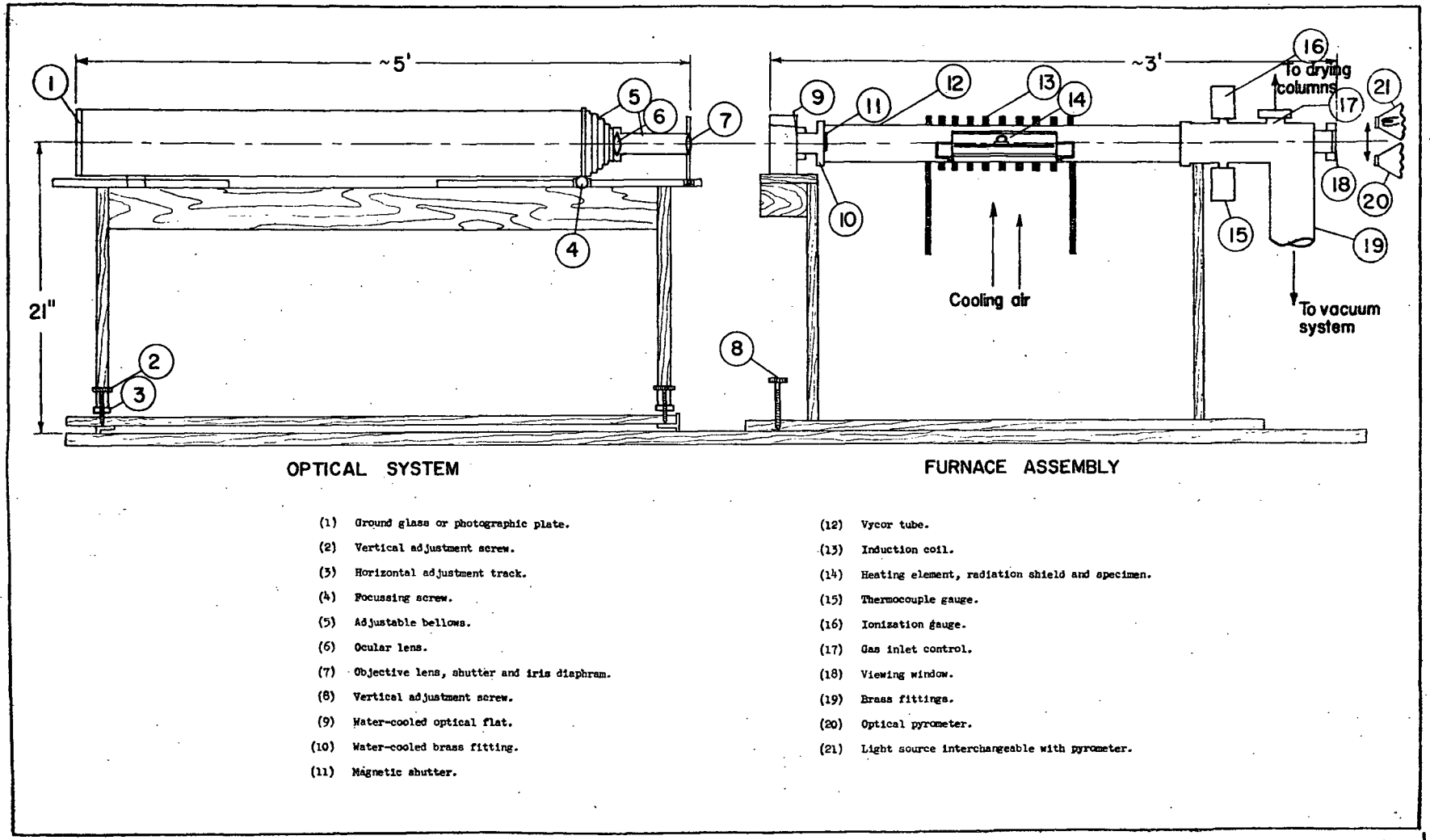

Fig. 4 Assembly drawing of the apparatus.

1. Furnace

The heating elements of the furnace were constructed from 0.005 inch molybdenum sheet (see Fig. 5). The susceptor consisted of a closed loop in the

Fig. 5. Molybdenum heating elements (dismantled) of the induction furnace.

form of a cylinder 0.75 inches in diameter and 3.5 inches long, open at both ends. A radiation shield surrounded the susceptor to prevent excessive heat loss. This shield consisted of an "open loop" cylinder 1.5 inches in diameter and 5 inches long, also open at both ends. The susceptor and radiation shield assembly was supported inside the induction coil by a molybdenum-rod framework. This rod was separated from the vycor tubing containing the heating elements by sintered alumina insulators.

The furnace-tube assembly consisted of a vycor (fused silica) tube, 2 1/2 inches in diameter and 18 inches in length. Rubber O-ring seals and silicone high vacuum grease were used in the vycor-to-brass joints at the end of the tube. At the camera end of the furnace, a water-cooled optical flat was

used to protect the camera lenses from heat radiation. Because of the high vapour pressures of metals at operating temperatures, a magnetic shutter was placed inside the furnace to protect the optical flat from metal vapours. At the other end of the furnace, a viewing window was built into the elbow leading to the vacuum system. Outside this window, a light source and an optical pyrometer were placed such that either could be positioned on the centre line of the furnace.

Through a water-cooled, copper induction coil (1/4 inch O.D.tubing, 21 turns) around the outside of the vycor tube, power was supplied to the heating element by a high-frequency induction generator. This unit, Lepel model T-10-3, produces power from 0 to 23.5 K.V.A. at 400,000 cycles per second. The power could be adjusted by varying either the plate current or the grid current in the tubes of the generator. Because of the low thermal capacity the furnace could be heated from room temperature to 1500°C in approximately three minutes and could be cooled from 1500°C to approximately 600°C in less than one minute, when the power input was lowered instantaneously. Both the rate of heating and cooling would follow logarithmic laws and at 1500°C the rate of heating would be much lower than the rate of cooling. The temperature in the furnace was measured to $\pm$5°C. by a Hartmann and Braun optical pyrometer, model TO-10-e. Emissivity corrections were not necessary because of the design of the susceptor. Power input to the furnace was limited by the loss of strength of the vycor tube at elevated temperatures. The tube was, therefore, air-cooled by means of a 10 inch diameter fan.

2. Vacuum system.

The pumping system was designed to produce a high vacuum or a controlled low vacuum. A mechanical fore pump and a two stage oil diffusion pump produced vacuums in the range of 10^{-4} to 10^{-5} mm. of Hg. With only the

fore pump operating, a reducing atmosphere could be continuously flushed through the system to maintain a vacuum of 0.5 mm. of Hg. The high vacuums were measured with a N.R.C. ionization gauge, type 507, and the low vacuums were measured by a N.R.C. thermocouple gauge, type 501.

Purified reducing atmospheres were obtained by continuously flushing dry hydrogen through the system. The hydrogen was supplied by Canada Liquid Air Co., Ltd. in 2,000 psi tanks. The purification and drying train consisted of a hydrogen 'deoxo' cartridge in series with columns of anhydrous calcium sulphate, silica gel, and phosphorous pentoxide. The 'deoxo' cartridge converted the oxygen impurity to water. The silica gel and anhydrous calcium sulphate reduced the water concentration in the hydrogen to 0.005 milligrams per liter of gas and the phosphorous pentoxide reduced the concentration further to less than 0.0002 milligrams per liter.

3. Optical system.

At temperatures above 1100°C, objects emit sufficient radiation to produce an outline image on a photographic film or ground glass plate. Sharp images of the incandescent drops in this investigation could be readily obtained at 1500°C if a camera were correctly designed for this purpose.

A camera was constructed to give a tenfold magnification. This was accomplished by the combination of a two-component objective lens (focal length of 27.5 centimeters) and a single component, ocular lens (focal length of 4.2 centimeters). The fixed objective lens was equipped with an adjustable shutter and iris diaphragm. The ocular lens was separated from the objective lens by a 10 to 15 inch adjustable bellows, and from the ground glass plate by a 42 to 48 inch adjustable bellows. The camera was positioned so that the optical axis was in the plane of the ceramic surface and parallel to the axis of the

furnace by means of vertical adjustment screws and horizontal adjustment tracks. Because of the length of the camera, sensitivity to vibrations was high and a very sturdy framework was necessary.

Focussing adjustments were made by means of a screw-thread adjustment on the ocular lens holder which moved parallel to the optical axis of the camera. Before the specimen was heated, preliminary focussing was accomplished with the aid of a light source at the far end of the furnace. The light source produced a silhouette of the specimen on the ground glass.

C. Preparation of Materials.

The single-crystal magnesium oxide was obtained as large irregular pieces such as shown in Fig. 6. These were cut into rectangular pieces roughly along $\{100\}$ planes with a Felker 'Di-Met' diamond saw. These rectangular pieces were annealed at 1000°C in order to facilitate[30] cleavage. After annealing, the crystals were cleaved by means of a small chisel and hammer into platelets approximately one centimeter square and one millimeter thick or into approximately square rods two to three centimeters long and 0.2 centimeter thick as

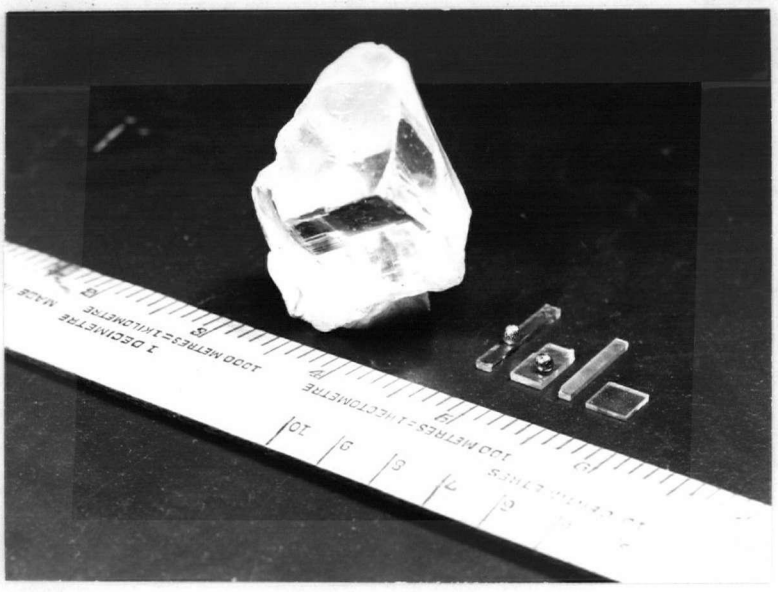

Fig. 6. Magnesium oxide 'as received' and cleaved crystals with and without nickel drops.

illustrated in Fig. 6. Whenever necessary, as discussed under experimental results, the cleaved platelets or rods were polished by immersion into hot phosphoric acid. A polishing time of one minute was sufficient to produce a microscopically smooth surface. Care was taken in handling the cleaved platelets and rods to avoid contamination of the surface and the introduction of plastic deformation. Metal tweezers were used whenever possible. To detect evidence of plastic deformation, as discussed under experimental results, a solution composed of 30 percent hydrochloric acid and 10 percent ammonium chloride was used.

The nickel in all experiments, but where mentioned, consisted of the Sherritt Gordon No. C525 rolled strip. This was cut into a small strip a few centimeters long and couple of millimeters wide. This was rolled up loosely to permit deoxidation on all surfaces. Where nickel powder was used it was compacted in a cylindrical die, 1/4 inch in diameter, under a pressure of forty tons per square inch. The compacting die was machined to form a compact of a shape required to insure an advancing contact angle.[11]

D. Experimental Procedure.

In all experiments but where mentioned, the following procedure was used: the metal was placed on the magnesium oxide platelet or rod inside the susceptor. With the aid of the light source, the specimen was levelled. The furnace was assembled and pumped to a fore pump vacuum of 5×10^{-3} millimeters of mercury. Purified hydrogen was then flushed through the furnace at a rate sufficient to maintain a vacuum of 0.5 millimeters of mercury. The temperature was slowly raised to approximately 800°C. Near this temperature, the hydrogen gas ionized and hydrogen-ion cleansing of the specimen took place. After a heating period of ten minutes, the power was turned off and the system was pumped down to a vacuum of 10^{-5} millimeters of mercury. The

power was again slowly increased until the temperature reached 1500°C as measured by the optical pyrometer. The specimen was maintained at this temperature for ten minutes. In the experiments to determine the wettability of the magnesium oxide by liquid nickel the image of the nickel drop was carefully focussed on the ground glass. The necessary dimensions to determine the wetting angle were made by means of a pair of calipers.

For the X-ray diffraction investigation to determine the formation of any compound or solid solution the nickel drops were sheared from the magnesium oxide. The layer of material adhering to the drop was scraped off by means of a small sapphire rod and prepared for identification by the X-ray powder method. The powder patterns were obtained by exposures to copper radiation (40 K.V., 15 m.a.) for two to five hours. These patterns were indexed and compared with patterns of standard materials recorded in the A.S.T.M. card index for powder patterns.

The preparation of specimens to investigate the diffusion of nickel into the magnesium oxide by means of X-ray fluorescence is described under experimental observations.

III. EXPERIMENTAL RESULTS

A. Observations on Interface.

Perpendicular and tapered sections of the magnesium oxide-nickel metal interface showed that the interface consists of a very sharp line. No evidence of any reaction product or intermediate phase could be found. Fig. 7 shows a tapered section of the interface at an apparent magnification of 4500x. The step in the interface is one of the higher cleavage steps, its height being approximately one micron.

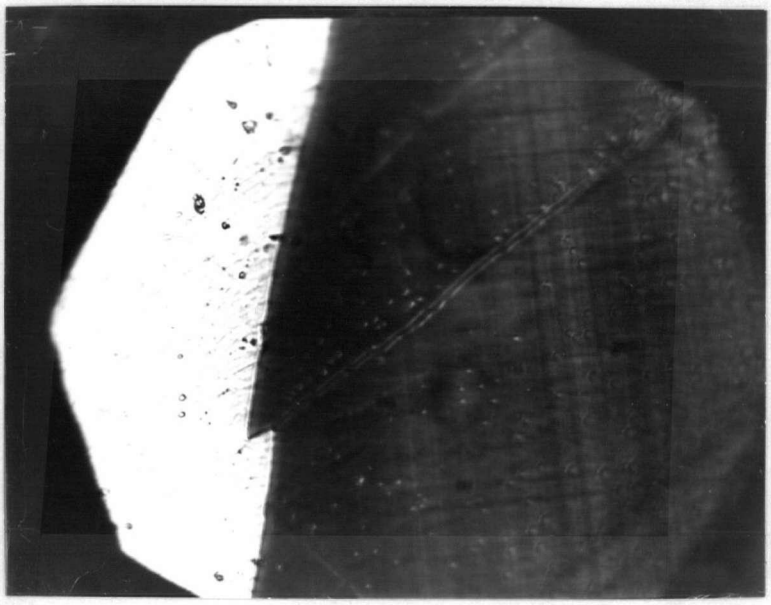

Fig. 7. Tapered section (1:6) of magnesium oxide-nickel metal interface (x750, apparent magnification is 4500x).

Fig. 8 shows a view obtained by looking through the magnesium oxide perpendicular onto the interface.

In addition to the cleavage steps, two perpendicular sets of parallel straight lines, also faintly visible in Fig. 7, can be seen. Their orientation corresponds to the $\langle 100 \rangle$ crystallographic directions of the magnesium oxide.

All the lines of both sets were observed to be continuous from one side of the interface to the other.

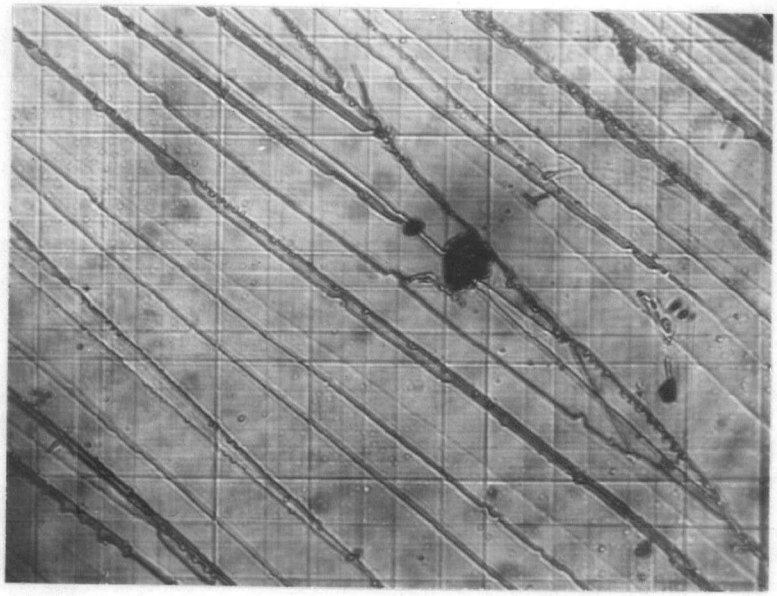

Fig. 8. Magnesium oxide-nickel interface as seen through the magnesium oxide (x250).

A dark field photomicrograph (see Fig. 9) shows in addition to the lines, a multitude of etch pits, some of them coincident with the lines.

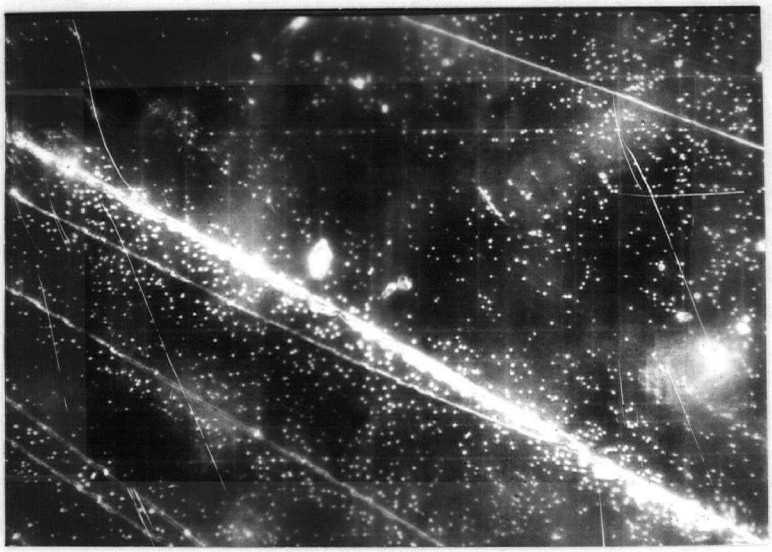

Fig. 9. Same as Fig. 8 but dark-field illumination (x250).

Fig. 10 shows the magnesium oxide-nickel interface at a magnification of 2500x. This magnification was achieved by mechanically polishing the platelet of magnesium oxide until a thin layer of magnesium oxide remained, such that at high magnifications the magnesium oxide platelet would not interfere with the focussing of the microscope. Most of the etch pits seem to be near cleavage steps indicated by the faint traces running diagonally across the figure.

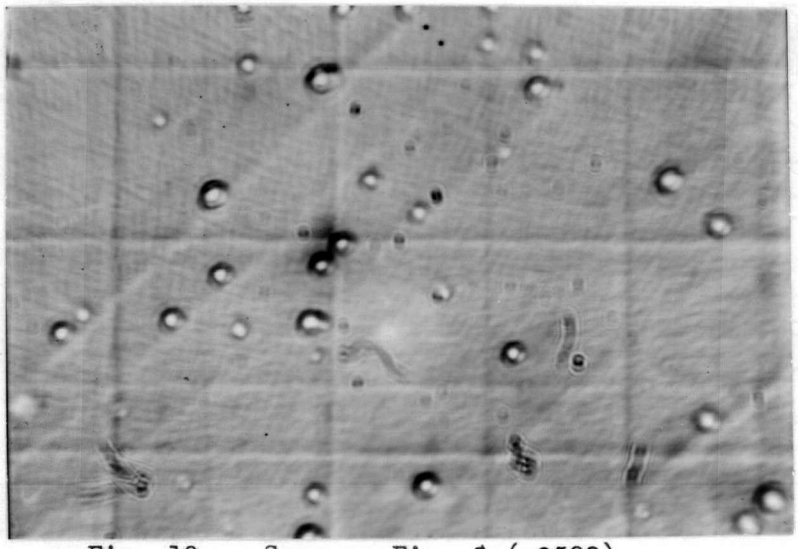

Fig. 10. Same as Fig. 8 (x2500)

To determine whether these lines were produced during cleavage or during the heating process, after cleavage a platelet of the magnesium oxide was polished by boiling in hot phosphoric acid until all surface irregularities, such as cleavage steps, were removed. A polishing time of approximately two minutes was sufficient.

Fig. 11 is a view of the interface between the polished platelet and a nickel metal drop located near the center of the platelet. It is clear that the lines can still be seen. A view near the edge of the platelet where the polishing was more severe, shows the lines to be curved, some even crossing others.

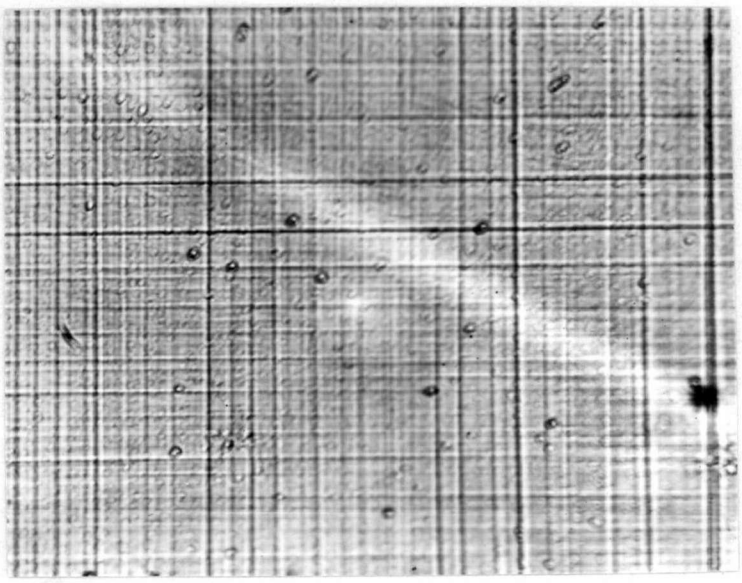

Fig. 11. Interface of nickel metal and magnesium oxide platelet polished before heating. Near center of platelet (x250).

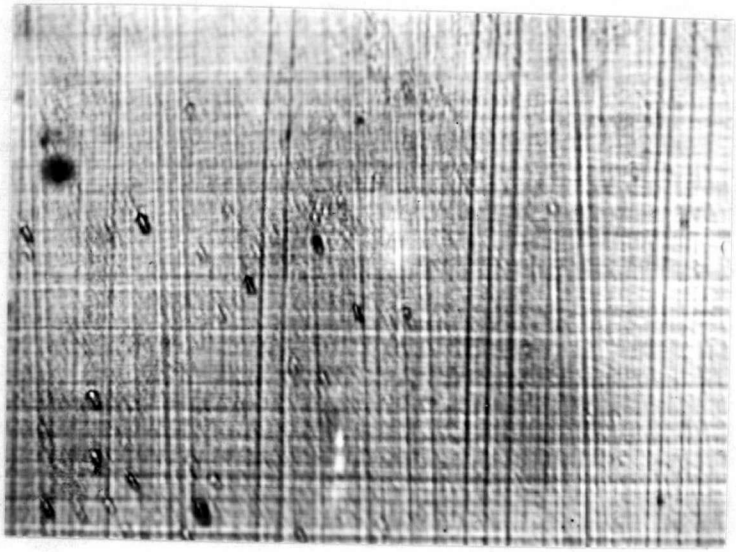

Fig. 12. Same as Fig. 11, but near edge of platelet where polishing was more severe (x250).

Examination of the interface between a nickel drop and a platelet, which was polished in hot phosphoric acid for approximately five minutes, showed that less lines seemed to appear on the interface than on the interface between a nickel drop and an unpolished platelet. No lines could be detected on the interface between a nickel drop and a platelet which was polished in hot phosphoric acid for approximately ten minutes.

Numerous specimens of platelets and rods with nickel metal drops were made to see if these lines could be made to appear on faces other than the interface between the magnesium oxide and nickel drop. The lines could be detected only on one specimen. On the side faces they were found to be parallel to the length of the rod. On the bottom face they were perpendicular to the length of the rod. Occasionally lines could be seen near the drop on the same cleavage face which supported the metal drop as shown in Fig. 16.

An attempt was made to see if the lines could be detected more easily by silvering the cleavage faces of the magnesium oxide, but this proved to be relatively unsuccessful as the silver did not adhere too well to the magnesium oxide in contrast to the beaker which contained the silvering solution. It was found that the silver did bring out the lines, but did not bring out any additional lines which could not be detected before silvering.

To see whether other metals would produce the lines, specimens were prepared with silver, copper, cobalt, aluminum and tin. The temperature was raised to approximately 50°C above the melting point of the respective metal. All metals, but the cobalt, which sheared off during the cooling, adhered to the magnesium oxide. In all cases no lines could be detected. However, heating the silver drop to 1400°C resulted in the formation of the lines. In contrast to the nickel-magnesium oxide interface the interfaces of silver, copper, aluminum and tin contained many gas occlusions.

A magnesium oxide platelet was heated and cooled without any metal drop. A drop of mercury was then placed upon the platelet and the interface examined for lines. The same was done using indium and gallium. In all three cases no lines could be found.

A nickel drop was melted on a rod of magnesium oxide and kept at 1500°C till the drop was evaporated away completely. On cooling no lines could be observed on the previous location of the drop.

A nickel drop was melted on a platelet of magnesium oxide and heated to 1800°C. Examination of the interface on cooling revealed no difference in the lines such as width or density compared with the line structure formed on cooling from 1500°C.

An attempt was made to see if any relationship might exist between lines on the interfaces between platelets on opposite sides of a cleavage crack and nickel drops. One example could be found where a one-to-one correspondence seemed to exist between approximately six neighboring lines.

To check if any one-to-one correspondence might exist between lines on the interfaces between different drops and the same crystal, a specimen was made which consisted of a cleaved rod supporting four drops of nickel metal. However, no evidence of a one-to-one correspondence could be detected.

To see whether the size of platelet has any effect on the nature of the lines, such as density, a nickel drop was melted on a platelet of magnesium oxide cleaved to a thickness of approximately 1/4 inch. Examination of the interface showed that the number of lines seems to be approximately the same as for thinner platelets.

In order to determine the effect of the cleavage steps on the nature of the lines a rod was selected which on one face had only two cleavage steps. When the interface was examined after a nickel drop was melted on it, no lines, such as shown in Fig. 8, could be detected. However, as shown in Fig. 13, faint <100> traces can be seen.

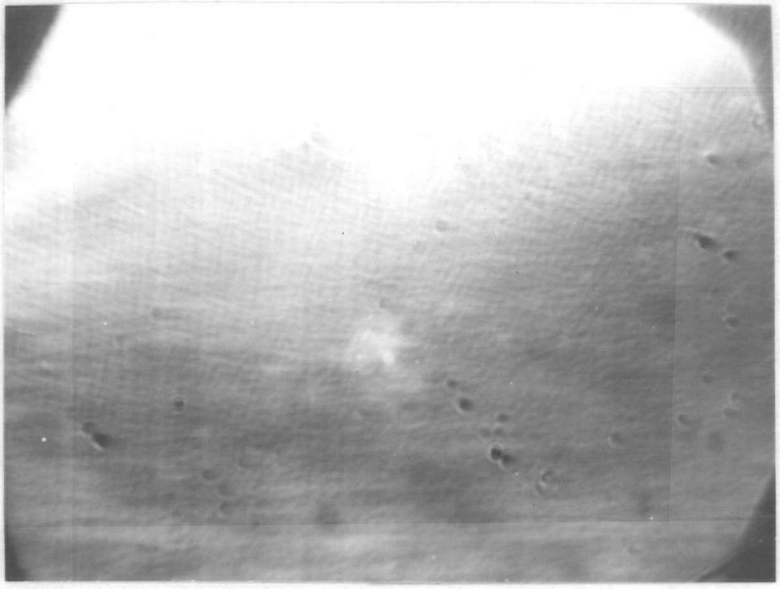

Fig. 13. Interface between nickel drop and platelet of magnesium oxide without cleavage steps (x300).

In only two of the many specimens made, evidence of cracking in the magnesium oxide could be detected. This took the form of <100> and <110> cracks extending from the top surface approximately half way into the platelet. In one case the drop was surrounded by an octagon of cracks composed of four <100> cracks and four <110> cracks.

B. Heating Rate.

To study the effect of the rate of heating and cooling, a platelet of magnesium oxide with a nickel drop was subjected to a number of heating cycles, in each cycle heating and cooling faster than in the previous one. Figs. 14 and 15 show the same area of the interface after the first and second

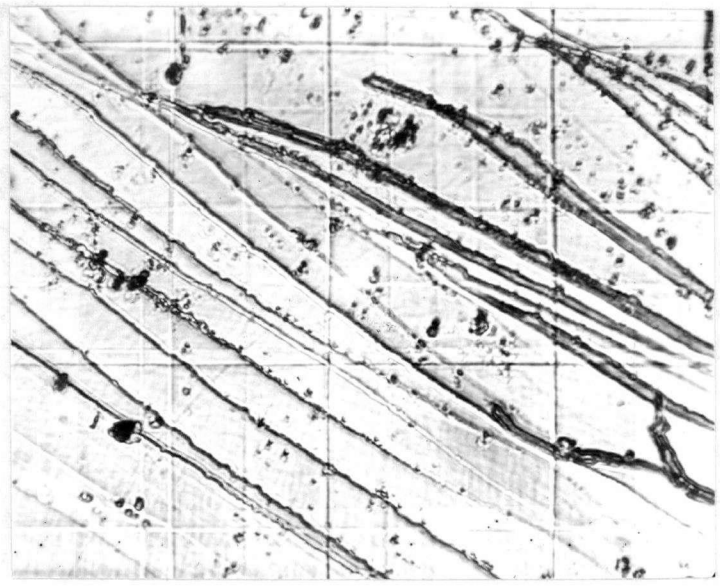

Fig. 14 Magnesium oxide-nickel interface after first slow heating cycle (x250).

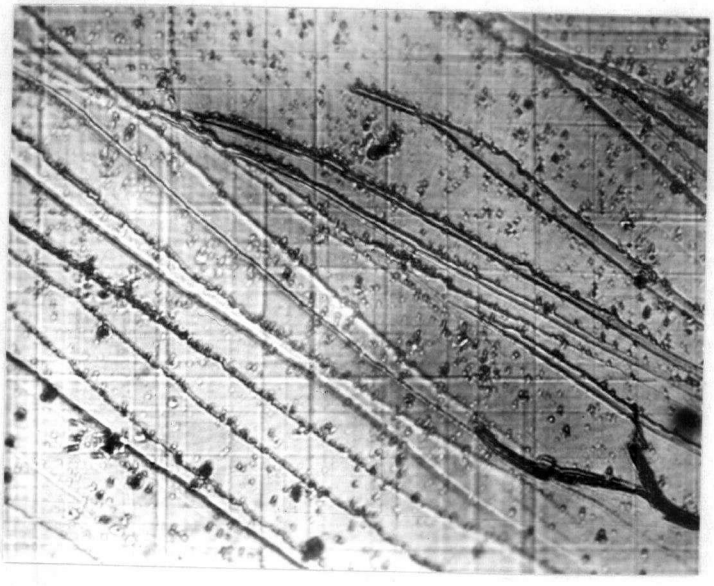

Fig. 15. Same area of interface as in Fig. 14 after second faster heating cycle.

heating cycle. In the first cycle the temperature was raised to 1500°C in approximately ten minutes, while cooling took approximately fifteen minutes. In the second cycle both these times were halved. By comparing both figures it can be noticed that during the second heating cycle additional lines appeared. In a third cycle, in which the temperature was raised in approximately three minutes and lowered by instantaneously switching off the power, no additional lines could be detected. Repetition of these experiments showed that these results were reproducible.

To study the effect of thermal cycling on the lines, a platelet with drop was subjected to fifteen heating cycles each time raising and lowering the power instantaneously. The interface was observed after the first, fifth, tenth and fifteenth cycle. No change in the lines such as width or intensity could be detected.

To subject the magnesium oxide to high thermal shock a rod without metal drop was heated to 1850°C and cooled quickly by lowering the power input instantaneously. Another rod was heated (in air) to a cherry red and immediately plunged into liquid nitrogen. On both rods a few lines appeared all running along the length of the rods. No evidence of fracture could be detected.

C. Etching by Liquid Nickel.

Figs. 16 and 26 show evidence of attack of magnesium oxide by liquid nickel as indicated by the concentric curves along the perimeter of the drop. In an experiment where a nickel drop was evaporated completely from a platelet the former location of the drop showed many concentric rings. Other evidence for attack is the occurrence of etch pits as shown in Figs. 9 and 12.

It was found that liquid nickel also attacks magnesium oxide at subgrain boundaries but this cannot be detected visually unless the magnesium

oxide and the nickel are held at 1500°C for at least thirty minutes.

D. Polarized Light.

The use of polarized light revealed the existence of internal strain. Fig. 16 shows the interface between a drop and a rod of the magnesium oxide. A similar pattern is obtained viewing the interface between a drop and a platelet. No such pattern could be detected with a platelet 1/4 inch thick.

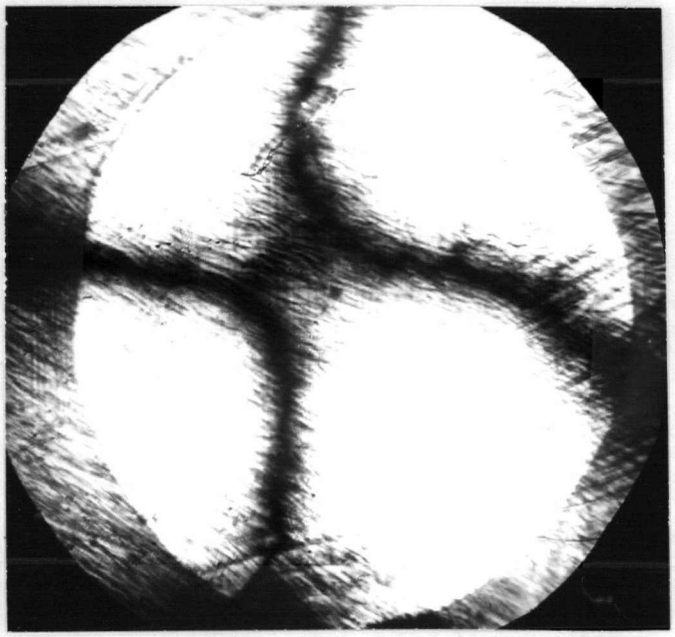

Fig. 16. Interface between nickel drop and rod of magnesium oxide under polarized light (x25)

As shown in Fig. 17 the side face of a rod in the vicinity of the drop revealed in addition to an overall pattern, as indicated by the two curved bands, an array of individual narrow bands oriented in $\langle 110 \rangle$, some extending nearly to the opposite face. No evidence of strain could be detected in the vicinity of the drop on the magnesium oxide rod which did not possess any cleavage steps.

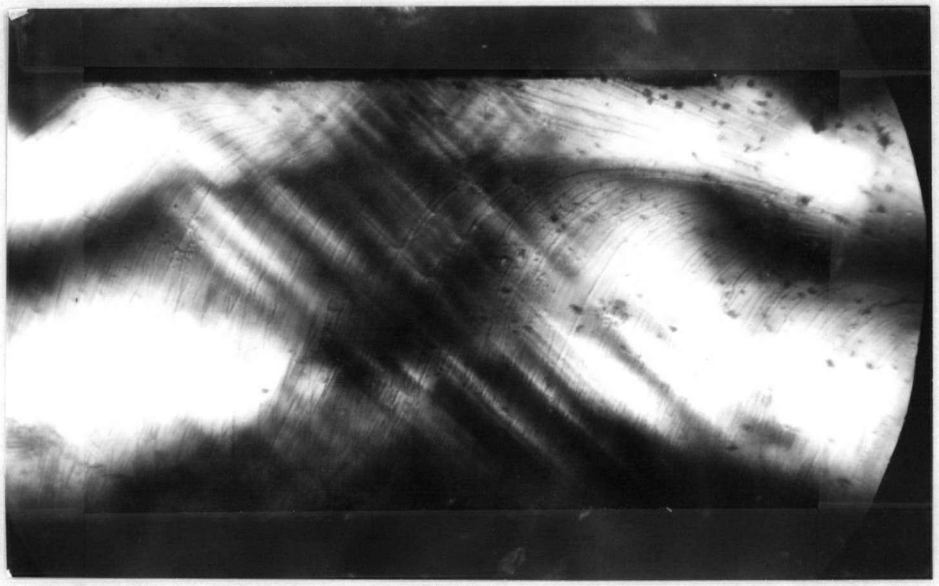

Fig. 17. Side face of magnesium oxide rod with nickel drop on top surface under polarized light (x25)

E. Chemical Etching.

Magnesium oxide platelets were chemically etched to bring out dislocations, subgrain boundaries and any plastic deformation. Fig. 18 shows

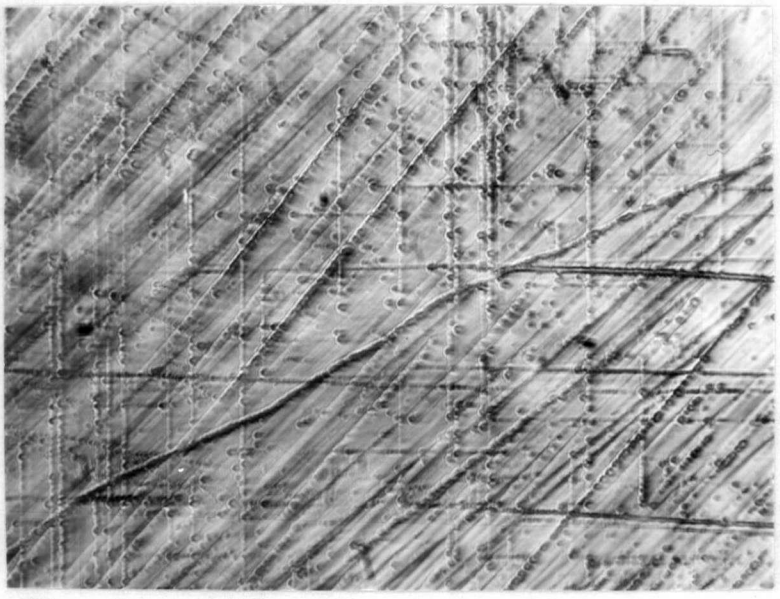

Fig. 18. Chemically etched cleavage face of magnesium oxide (x100)

an etched platelet with an array of two perpendicular sets of parallel rows

of etch pits oriented in $\langle 100 \rangle$. The diagonal line from the lower left to middle right is a subgrain boundary. The other lines running approximately in a $\langle 110 \rangle$ direction are the remains of cleavage steps.

Fig. 19 shows a high density of etch pits near one of the higher cleavage steps. It may be noticed that the etch pits seem to be in a broad band parallel to the cleavage step.

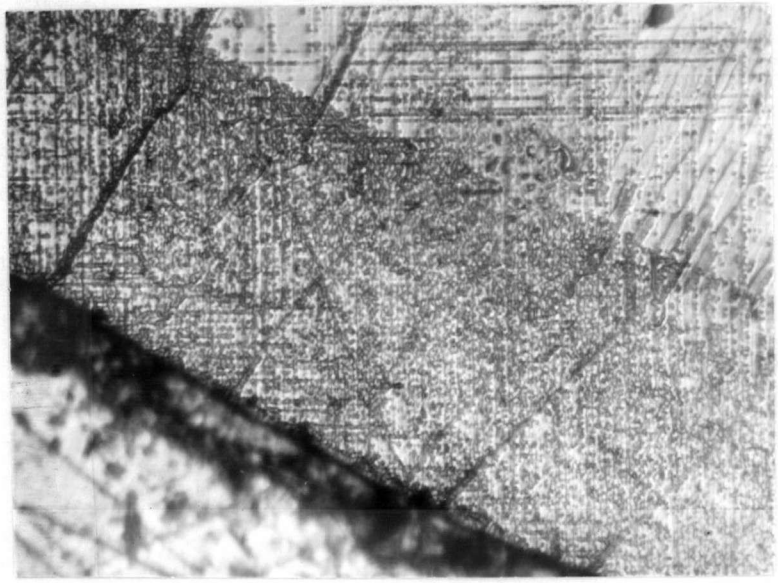

Fig. 19. Chemically etched cleavage face, near high cleavage step (x100).

In examining many etched crystals it was found that the occurrence of arrays of etch pits such as shown in Fig. 19 are relatively rare, many crystals not having any. Platelets cleaved from crystals, which were not annealed, have more of these $\langle 100 \rangle$ rows of etch pits than platelets cleaved from annealed crystals. A rod which did not have any cleavage steps on one face did not show any arrays of $\langle 100 \rangle$ etch pits.

To examine the nature of these arrays of etch pits the crystal of Fig. 18 was continuously etched and observed at intervals. It was found that the etch pits making up the arrays became deeper and larger, then became flat bottomed and finally disappeared altogether. Most of the etch pits

became flat bottomed when a few microns deep, the deepest being approximately from five to ten microns deep. The shortest distance between two neighboring etch pits was approximately one and a half to two microns.

It was also observed that these <100> arrays of etch pits seemed to be etched faster than grown-in dislocations or subgrain boundaries. Etching the crystal which was opposite the crystal of Fig. 18 at cleavage showed that the same etch pits do not occur (see Fig. 20). This has also been observed in

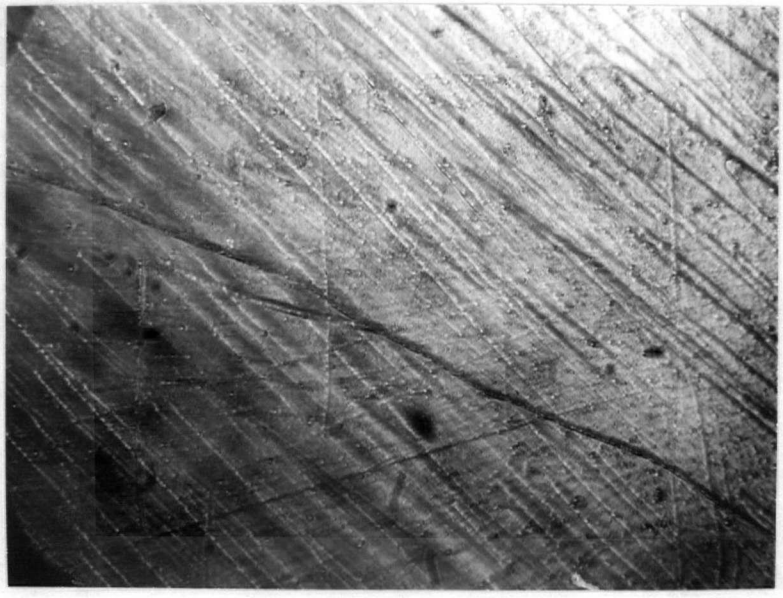

Fig. 20. Opposite cleavage face from Fig. 18 (x100).

many other crystals. Similar arrays of etch pits are visible in Fig. 9.

To see whether the existence of these arrays of etch pits is a condition for the formation of lines, a nickel drop was melted on a platelet of magnesium oxide which after a light etch showed subgrain boundaries but no evidence of etch pits. Observing the interface showed the existence of these lines with a line density comparable with that of Fig. 8.

To see whether a relationship exists between the etchpits produced

by chemical etching and the lines produced when a nickel drop is melted on a platelet, a platelet was given a light etch until etch pits appeared. A nickel drop was then melted on the platelet and the lines under the drop were then compared with the etch pits in the same area. Fig. 21 shows the platelet after chemical etching. Fig. 22 shows the same area, as seen through the platelet,

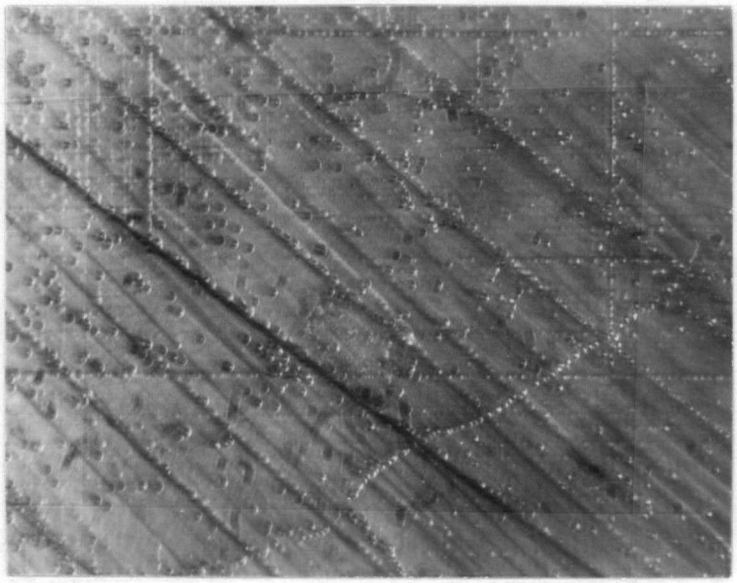

Fig. 21. Etched cleavage face of magnesium oxide. (x100)

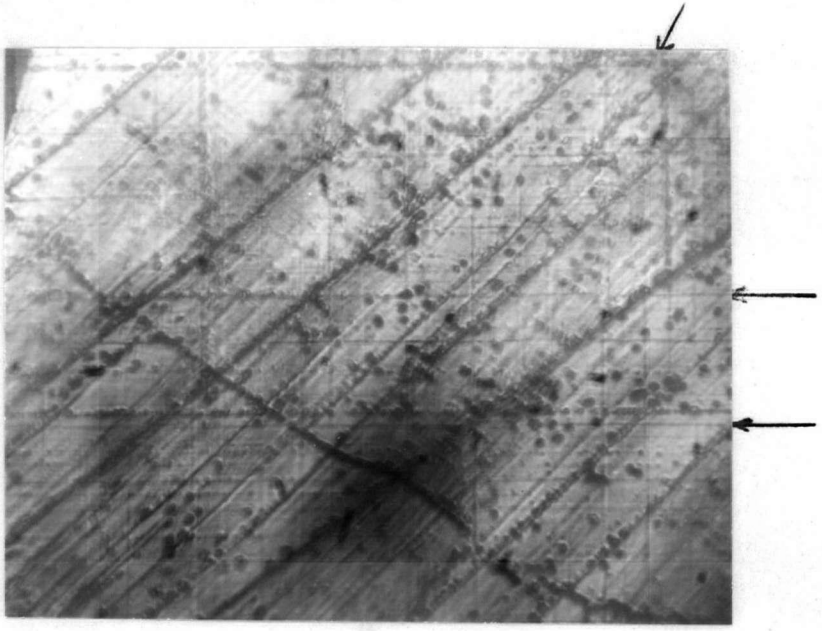

Fig. 22. Same area as in Fig. 21 but with nickel drop, as seen through the platelet, and therefore its mirror image (x100).

after a nickel drop was melted on it. Two examples can be found where a line continues at the end of a row of etch pits. In addition, a line can be seen to go through two single etch pits, as indicated by the lower arrow. It can be seen that the presence of a subgrain boundary does not seem to interfere with the formation of the lines.

Chemical etching of a rod with a nickel drop covering the complete width of the top cleavage face revealed evidence of plastic deformation on all the other faces, but in the vicinity of the drop only. On the side faces two $\langle 110 \rangle$ traces of slip lines could be seen and traces of $\langle 100 \rangle$ slip lines parallel to the top surface could be seen. On the bottom face only $\langle 100 \rangle$ traces, oriented perpendicularly to the length of the rod, could be detected.

F. Nature of Deformation.

In order to compare the lines seen on the interface between the magnesium oxide and the nickel drop with the deformation of a plastically deformed magnesium oxide crystal, a rod was slowly bent by hand till fracture occurred. Fig. 23 illustrates the four faces of the rod at the fractured end. On the tension and compression sides of the rod the lines, which lie in (100),

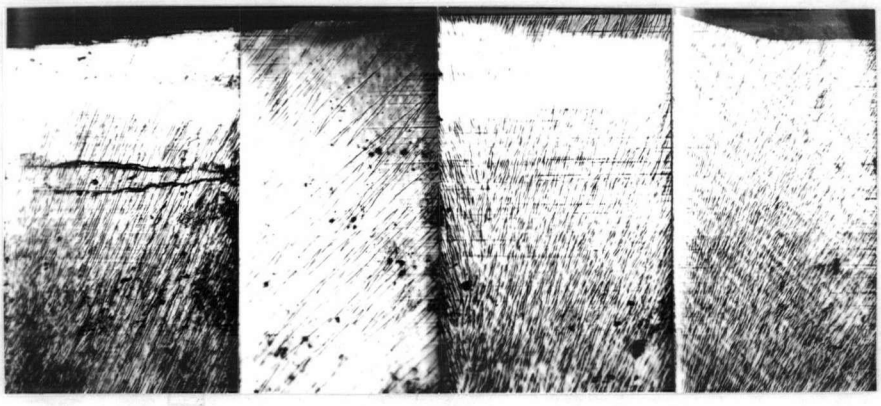

Fig. 23. Faces of broken rod of magnesium oxide near fracture end. Unetched (x15).

are more or less continuous across the face, whereas on the side faces the lines extend inward from the tension and compression faces gradually fading out towards the neutral axis.

Fig. 24 shows the same rod after etching. On the four faces additional <110> lines can be seen. As in the case of the <100> lines they are continuous across the tension and compression faces and on the side faces extending inward towards the neutral axis.

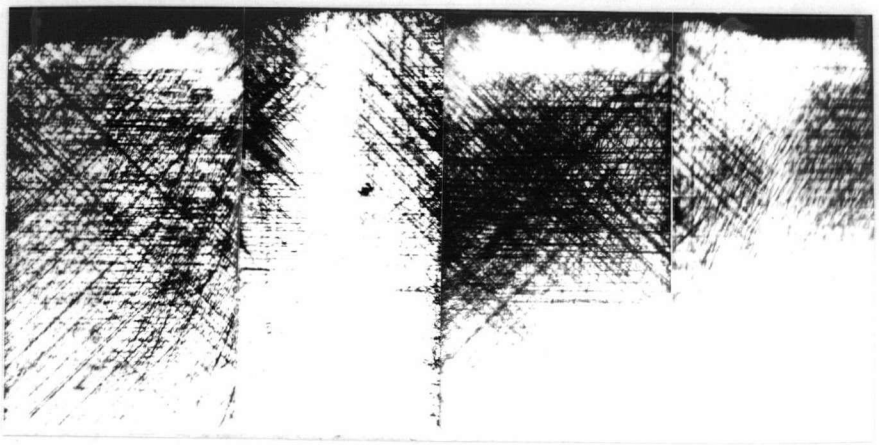

Fig. 24. Faces of broken rod near fracture end. Etched. (x15).

Examining a side face of the rod near the point of fracture with polarised light reveals arrays of bands oriented in <110>, as shown in Fig. 25.

In order to etch the interface between a nickel drop and a rod of magnesium oxide the drop was removed by melting it and allowing it to roll off the rod. The rod was then chemically etched. To check the effectiveness of the etchant, some plastic deformation was introduced deliberately in one end of the rod. Fig. 26 shows that no <110> traces can be seen on the former location of the drop. In the plastically deformed region of the rod <110> slip lines could be found, some of them extending into the former location of the drop showing that <110> slip lines could be etched.

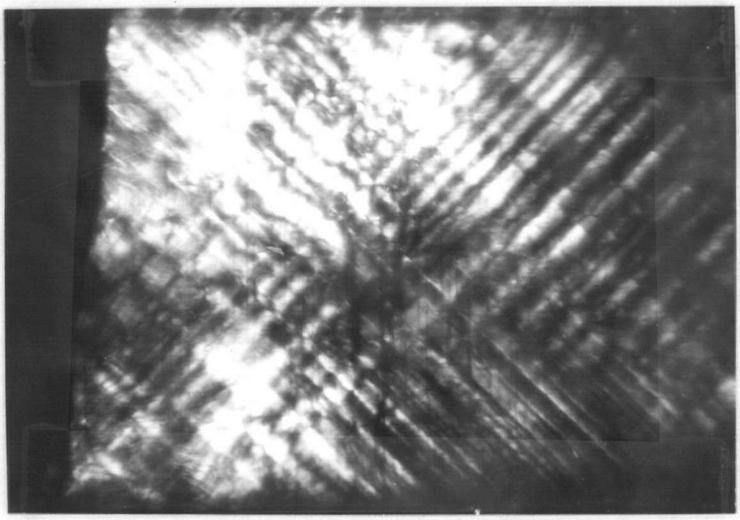

Fig. 25. End of broken rod under polarized light (x30).

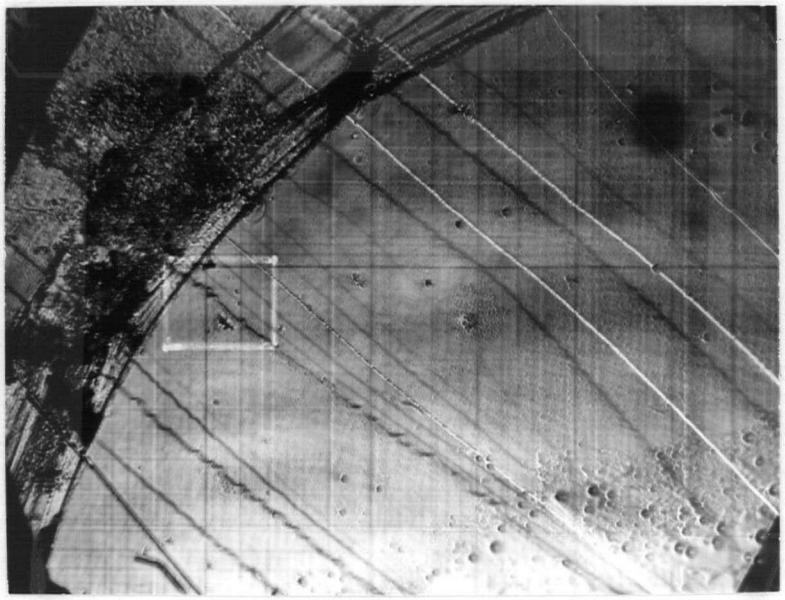

Fig. 26. Area on rod from which nickel drop was removed by melting. Unetched (x125).

It was observed that the usual fifteen minute etching time was not sufficient to bring out the $\langle 100 \rangle$ rows of etch pits, whereas after fifteen minutes the plastic deformation which was deliberately introduced showed up very clearly.

Fig. 27 also shows that little or no etching occurred near the perimeter of the former location of the nickel drop. Before etching, the lines were observed to be continuous to the perimeter as shown in Fig. 26.

Fig. 27. Same as Fig. 26. Etched thirty minutes (x750).

In bending the rods it was observed that those rod which possessed a face which was cut by the diamond saw were more ductile than those rods which possessed four cleavage faces. All of the rods which possessed a cut face could be bent to the degree as shown in Fig.28. Only a few of the

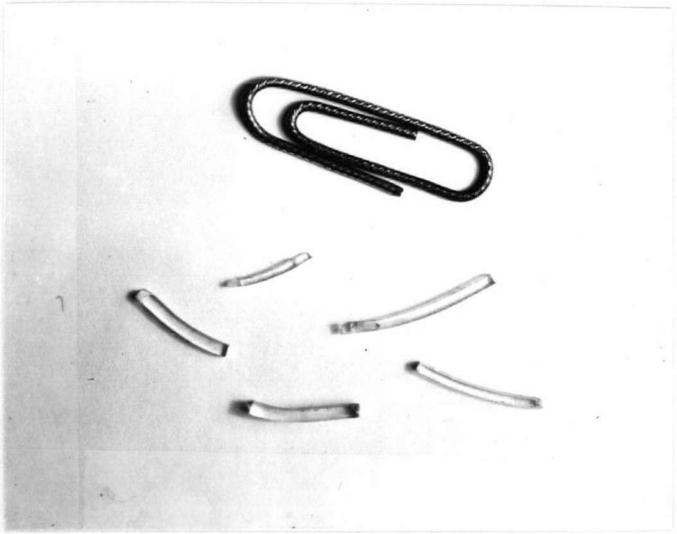

Fig. 28. Bent rods of magnesium oxide, illustrating ductility.

cleaved rods which possessed four cleavage faces were as ductile as this, most of them fracturing after a small amount of bending.

To examine the nature of fracture of a polished rod, a rod was polished in hot phosphoric acid for ten minutes after which it was fractured by bending. The rod was then chemically etched. The result is shown in Fig.29.

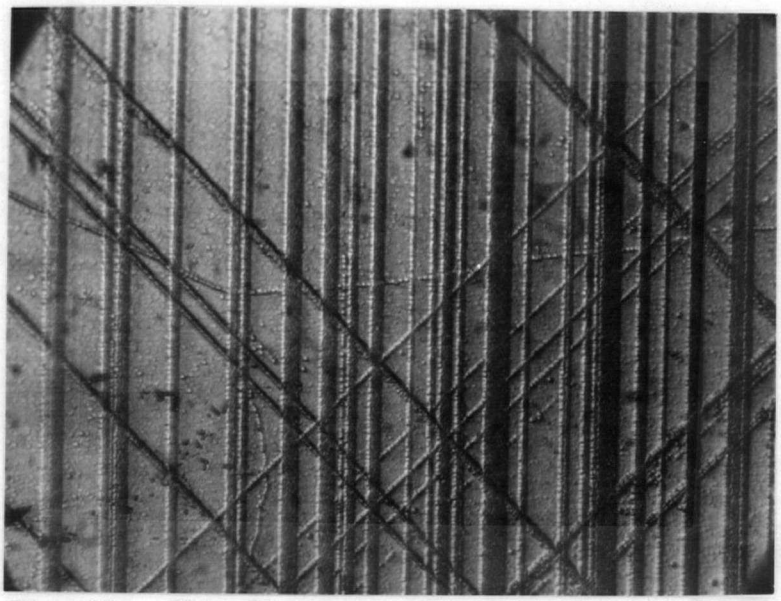

Fig. 29. Slip lines on polished and broken rod of magnesium oxide. Etched 15 mins. (x100).

Fig. 30 shows an area of the rod of Fig. 24. It can be seen that the traces

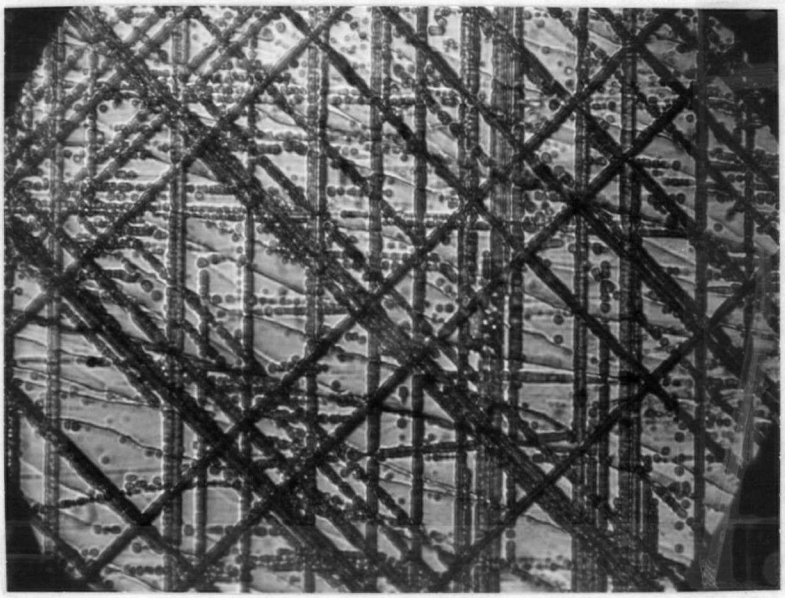

Fig. 30. Slip lines on unpolished magnesium oxide rod. (x100)

in the polished rod are of a different nature than the traces in the unpolished rod.

G. Strength of Bond

To test the strength of the bond formed between the nickel metal and the magnesium oxide cleavage face, a drop was sheared from a platelet to see where fracture would occur. Fig. 31 shows the fracture surface of the drop. By the two sets of cleavage steps it can be seen that fracture occurred through the magnesium oxide.

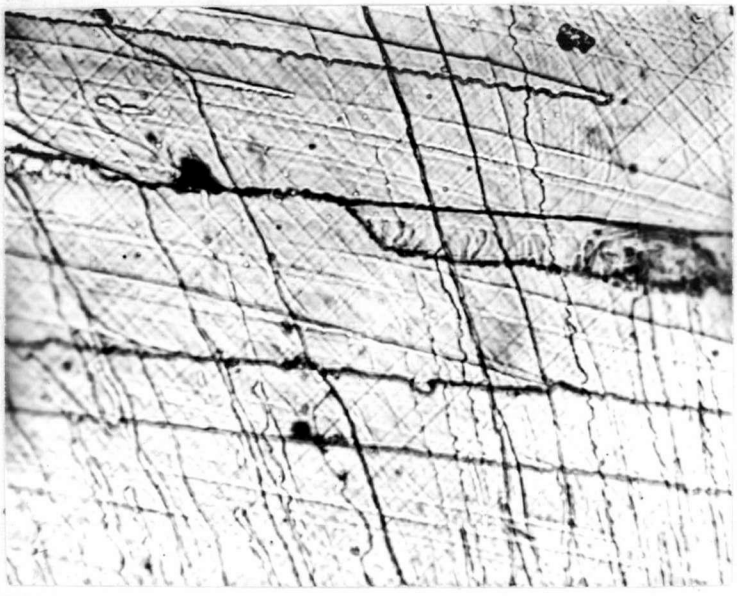

Fig. 31. Fracture surface between nickel drop and magnesium oxide platelet. (x250).

A perpendicular section through the drop showed that the layer of magnesium oxide sheared off with the drop was approximately twenty microns thick.

A drop of nickel composed of Sherritt Grade C 525 and 2 percent nickel oxide was sheared from the magnesium oxide. Fracture occurred at the interface rather than through the magnesium oxide.

A drop of nickel was melted on a platelet of magnesium oxide by

bringing the temperature up to the melting point of nickel and holding it there approximately ten seconds after the nickel melted. Shearing the drop from the platelet revealed that fracture occurred mainly at the interface and occasionally through the magnesium oxide.

H. Debye-Scherrer X-ray Analysis of Interfacial Material.

X-ray analysis of the interfacial material was made by the Debye-Scherrer powder method. Three materials were investigated:

1. the interfacial material between magnesium oxide and Sherritt C 525 nickel held at 1500°C for one hour. Here evidence was found for the existence of a magnesium nickel compound. No evidence could be found for the presence of nickel oxide or magnesium. (For powder patterns and calculations see Appendix I).

2. the interfacial material between magnesium oxide and Sherritt C 525 nickel to which 2% nickel oxide had been added. Here only nickel and nickel oxide could be detected. No evidence for the existence of magnesium oxide could be found, supporting the experimental observation that when removing the drop from the magnesium oxide, fracture occurred at the interface rather than through the magnesium oxide as happens when removing a drop of pure nickel from magnesium oxide. (For powder pattern and calculations see Appendix II).

3. the top layer of the magnesium oxide from which the nickel drop had been removed by melting. No evidence for the presence of nickel or magnesium-nickel compound was found.

I. Diffusion of Nickel into Magnesium Oxide.

The relative amounts of nickel which diffused into the magnesium oxide while at 1500°C were determined by removing the nickel drop from the

magnesium oxide and by determining the amount of nickel by measuring the intensity of the nickel K-α line by X-ray fluorescence. The specimens were prepared by taking two rods from opposite sides of a cleavage crack. Nickel drops of equal weight were then melted on them. One specimen was brought to 1500°C, then cooled so as to introduce plastic deformation (see under Discussion) and again brought to 1500°C and held at this temperature for fifteen minutes. The other specimen was just brought to 1500°C and held there for an equal length of time.

Enough specimens were prepared such that the drops could be removed from the rods in three ways:

1. forcible removal by means of shearing them off.
2. by melting and allowing them to roll off.
3. by holding the specimens at 1500°C till all the nickel had evaporated away.

The remaining rods were then placed into the X-ray fluorescence machine and the relative intensities were plotted graphically. The relative peak heights are an indication of the relative quantities of nickel in each rod. The results for removal of the nickel drops by shearing and melting are illustrated in Fig.32. In the rods from which the nickel drops were evaporated only a trace of nickel could be detected, which were in approximately equal amounts.

J. Wettability

The results of the determination of wetting angles between various nickel materials and magnesium oxide in the polished or 'as cleaved condition' are shown in Table III. The wetting angles were calculated from the drop dimensions. Measurements were made approximately 1 minute and 20 minutes after the nickel melted. In the case of the Sherritt C525 + 2% NiO, it was observed

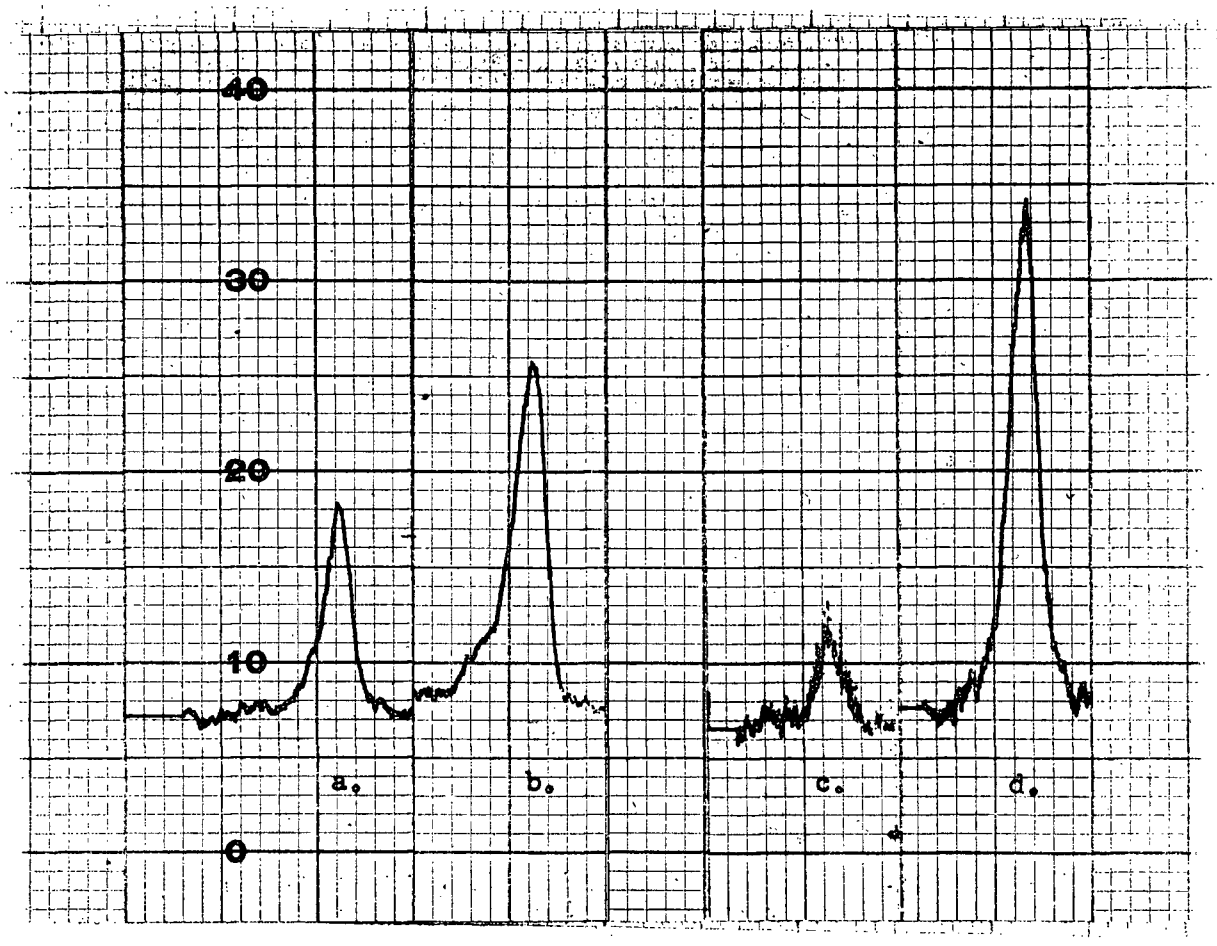

Fig. 32. Relative amounts of nickel as indicated by intensity of nickel K-α line. (Relative peak heights indicate relative amounts).

a. Drop melted off. (Undeformed rod)
b. Drop melted off. (Deformed rod)
c. Drop sheared off. (Undeformed rod)
d. Drop sheared off. (Deformed rod).

that immediately upon melting, the nickel oxide segregated at the surface of the drop and formed what seemed to be a solid coating around the liquid nickel. After approximately thirty minutes this coating had disappeared but for an occasional piece which could be seen to rotate around the drop. This was thought to be due to the stirring effect by the applied magnetic field.

TABLE III

Wettability Results.

Wetting angle in degrees

	Polished		'As cleaved'	
	time after melting (min.)		time after melting (min.)	
Material	1	20	1	20
Sherritt C grade No.525	102.1	104.6	103.6	98.9
High purity nickel	107.4	103.8	101.6	103.2
Carbonyl	114.5	95.5	108.3	102.2
Sherritt high sulphur	103.6	99.1	102.1	102.0
Sherritt C grade + 2% NiO	78.0	87.2	102.0	97.0

A large hysteresis of wetting was observed when a nickel drop was evaporated from the magnesium oxide. The estimated wetting angles varied between approximately 105° and 80°. During evaporation the wetting angle would decrease till a sudden contraction occurred at which the wetting angle would change discontinuously from a lower to a higher value. (For calculation of wetting angle see Appendix III).

IV. DISCUSSION

A. Plastic Deformation.

Comparing the results obtained by plastically deforming a rod by bending and the line structure, as observed on the interface, one can conclude that the magneium oxide is plastically deformed during some part of the heating cycle when melting a nickel drop on a crystal of magnesium oxide (see Section C).

The main evidence supporting this -

1. Identical orientation of the observed lines and the slip lines on the plastically deformed rod.

2. Identical $\langle 110 \rangle$ patterns can be seen when the interface and the surface of the plastically deformed rod are examined with polarized light (see Figs. 17 and 25).

B. Nature of the Plastic Deformation.

Shown in Fig. 33 are the slip systems in magnesium oxide. It can be seen that there are four slip planes inclined at 45° to the cleavage plane and will henceforward be referred to as $(110)_{45}$ planes.[18] In addition there are two slip planes at 90° to the cleavage plane and will be referred to as $(110)_{90}$ planes.

The lines of intersection between the four $(110)_{45}$ planes and the cleavage plane lie in $\langle 100 \rangle$ directions. The two $(110)_{90}$ planes intersect the cleavage plane in two orthogonal $\langle 110 \rangle$ directions.

The corresponding Burger's vectors, which indicate the slip direction for each plane, are indicated by the arrows.

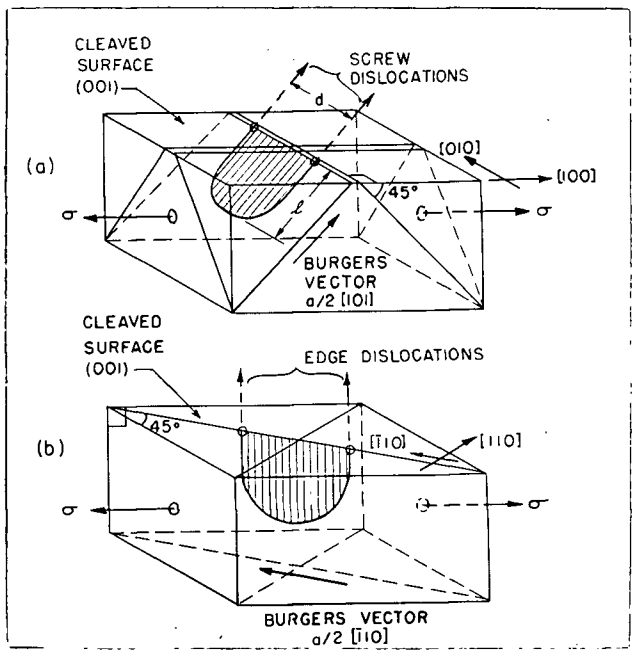

Fig.33. Slip systems in magnesium oxide.

a. Screw dislocations
b. Edge dislocations.

It is clear that the plastic deformation under the nickel drop takes place by slip over $(110)_{45}$ planes only. No slip occurs over the two $(110)_{90}$ planes as indicated by the evidence in Fig. 27. Here no $\langle 110 \rangle$ traces of etch pits can be seen. These $\langle 110 \rangle$ traces would be expected if slip had occurred over the $(110)_{90}$ planes as dislocations would intersect the surface and would show up on etching.

The fact that slip takes places over all four $(110)_{45}$ planes, is shown in Fig. 12 where, due to uneven polishing, the slip lines intersect on the surface, which is an indication that these slip lines are caused by slip on different planes. On the bent rod slip occurs on two $(110)_{45}$ and two $(110)_{90}$ planes. No slip occurs on the remaining $(110)_{45}$ planes as their Burger's vectors are oriented perpendicular to the stresses.

From Figs. 16 and 17 and the fact that slip lines can be detected on the other cleavage faces in the vicinity of the drop only, it can be

concluded that the presence of the drop is essential for plastic deformation to take place.

C. Cause of the Plastic Deformation.

The stresses responsible for the plastic deformation can be produced in two possible ways:

1. The difference in contraction on cooling between the magnesium oxide and nickel or any compounds formed at the interface can cause stresses high enough to deform the magnesium oxide plastically.

2. By thermal stresses. Thermal stresses are due to differences in expansion in different parts of one body caused by temperature gradients set up during heating or cooling.

The first possibility is unlikely when using nickel drops. A calculation (see Appendix IV) shows that the difference between the coefficients of thermal expansion of magnesium oxide and nickel is too small to cause stresses high enough to exceed the yield stress. It is felt also that even when the stresses due to thermal contraction were high enough, the drop would have sheared off completely, as in the case of cobalt.

From the various experiments described under experimental results, it can be seen that thermal stresses can cause plastic deformation in magnesium oxide. The fact that additional slip lines occur when a platelet with drop is heated and cooled faster at a second cycle is not sufficient evidence that thermal stresses are responsible for the plastic deformation. It may well be possible that the plastic deformation in the first cycle produces additional slip sources which are then activated during the second cycle. However, the fact that a silver drop when heated to 1400°C causes plastic deformation

whereas no evidence of plastic deformation can be found when the silver is heated to 1000°C is conclusive evidence that thermal stresses are responsible as a liquid is not capable of exerting forces other than gravitational. In addition, a calculation of the possible magnitude of the thermal stresses shows that a small temperature difference between the center and the perimeter of the interface between the nickel drop and the magnesium oxide can give rise to stresses exceeding the yield stress (see Appendix V).

From the fact that no lines could be detected on the area of the magnesium oxide platelet from which the drop had been evaporated can be concluded that the plastic deformation takes place during the cooling. This is also supported by the fact that the rate of change of temperature is substantially higher on cooling than on heating as discussed under equipment.

D. Temperature at which Plastic Deformation Occurs.

An actual measurement of the temperature at which the plastic deformation occurred could not be made, but it is felt that the plastic deformation took place immediately when cooling began, therefore at a temperature of practically 1500°C. This is reasonable when one realizes that the region under the drop can lose heat by conduction only and then when areas other than the area under the drop have cooled down. Furthermore the rate of heat loss at these areas occurred by radiation only and will therefore be high at these temperatures.

E. Plastic Deformation During Heating.

The only way that plastic deformation could occur during heating is if the nickel drop, but not the magnesium oxide, were heated suddenly. It was observed that the nickel supercools at least 50°C, indicated by the experimental

observation that the drop suddenly 'flashed', due to the heating of the drop by the sudden release of the heat of melting. This in effect, corresponds to an infinite heating rate and could give rise to thermal stresses in the magnesium oxide which exceed the yield stress.

However, from the experimental observation that a drop of silver melted on a platelet of magnesium oxide can give rise to plastic deformation at temperatures above the melting point of silver, one can conclude that the supercooling effect is not responsible.

F. Study of the Plastic Deformation Under Polarized Light.

The use of polarized light shows that, after cooling, stresses exist in both the platelets and the rods in the vicinity of the nickel drop.

Comparison of the patterns shown in Figs. 16 and 17 with patterns published by Jessop and Harris[31] shows that the pattern in Fig. 16 is similar to the pattern of a photoelastic model of a vertical circular plate loaded by a vertical compressive force. The pattern in Fig. 17 is similar to the elastic strain pattern of a photoelastic model of a beam loaded at the center and supported at the ends.

G. Mechanism of the Plastic Deformation.

It is felt that the rods and platelets were deformed in the following way: Initially at 1500°C both drop and platelet or rod are at the same temperature. When the temperature is lowered, the region under the drop does not cool as fast as the rest of the platelet or rod. This gives rise to thermal stresses. They will be in the form of compressive and shear stresses (see also Appendix V). As the yield stress of the region under the drop, because of the higher temperature, is lower than the yield stress elsewhere in

the platelet or rod, it will plastically deform whenever the thermal stresses exceed the yield stress. Upon further cooling the deformed region will contract more than the rest of the platelet and will give rise to the overall elastic bending moment as seen in Fig. 17. Upon cooling no additional plastic deformation will take place as the yield stress is higher at lower temperatures.

As the region under the drop will be compressed when deformed, it will be under tension once the drop and platelet are at room temperature. This is supported by the fact that occasionally cracks can be seen around the perimeter of the drop.

Although the region under the drop is in tension and therefore the opposite face under compression, the overall strain is that of a beam supported at its ends and loaded at its center, because on cooling the region of the rod or platelet under the nickel drop contracts more than elsewhere.

The fact that a bending moment exists in the rods is also supported by the evidence in Fig. 16, which shows an elastic strain pattern identical to the pattern obtained in a vertical circular plate under a vertical compressive load. The experimental observation that a pattern such as in Fig. 16 could not be detected on the interface between a nickel drop and a platelet 1/4 inch thick, can be explained by the fact that the strain resulting from the bending moment in a thick platelet is less than in a thin platelet.

It is felt that little or no contribution is made to the stresses in the magnesium oxide by the differences in contraction on cooling as the coefficients of thermal expansion are nearly identical. This is also supported by the experimental observation that no evidence of strain could be detected in the vicinity of the drop melted on the rod which did not possess any cleavage steps.

H. Temperature Dependence of the Plastic Deformation

The fact that no plastic deformation could be detected on the interfaces between platelets of magnesium oxide and drops of copper, aluminum and silver heated to approximately 50°C above the melting point of the respective metal can be explained by the fact that the yield stress of magnesium oxide is higher at these temperatures than at 1500°C. In addition, as the thermal stresses induced in the magnesium oxide will be a function of the rate of cooling and as cooling takes place by radiation only and therefore depends on the fourth power of the temperature, the thermal stresses at lower temperatures will be substantially lower and may be low enough not to exceed the yield stress of the magnesium oxide.

I. Nature of Slip Sources.

As the slip lines coincide with rows of $\langle 100 \rangle$ etch pits as shown in Figs. 9, 21 and 22, it can be concluded that the lattice imperfections which give rise to the etch pits are responsible for the slip sources in magnesium oxide. This is substantiated by the fact that no slip occurs on $(100)_{90}$ planes, although the thermal stresses present are high enough for slip to occur on these planes.

The etch pits are evidence of dislocation-loops in the screw orientation introduced in the surface during cleavage because:

1. They are line imperfections in the crystal as shown by the experimental observation that they continue into the crystal on continued etching of the surface.

2. Their orientation corresponds to the orientation of screw dislocations (see Fig. 33).

3. They appear only on one side of the cleavage crack as can be seen in Figs. 18 and 20 and are therefore introduced during cleavage.

4. They become flat-bottomed on continued etching showing them to be closed loops.[17]

5. They etch faster than subgrain boundaries and grown-in dislocations. This indicates that these dislocations are 'fresh' dislocations.[18]

Additional evidence for these dislocations to be 'fresh' are the etch pits in Fig. 9, produced by etching of the magnesium oxide by liquid nickel. These etch pits, as in the case of chemical etching, appeared faster than subgrain boundaries and grown-in dislocations. It is felt that all the etch pits shown in Fig. 9 are evidence of dislocations introduced during cleavage, although they do not appear in arrays.

J. Mechanisms of Introduction of Slip Sources into Surface.

The formation of $\langle 100 \rangle$ rows of dislocation loops is closely connected with the formation of cleavage steps as:

1. When chemically etching a cleavage face no rows of $\langle 100 \rangle$ dislocations can be detected when the cleavage face does not display cleavage steps.

2. A high density of $\langle 100 \rangle$ rows of etch pits is produced near high cleavage steps as shown in Fig. 19.

3. The etch pits produced by the liquid nickel as in Fig. 10 seem to be near low cleavage steps and

4. Many of the rows of dislocations terminate on cleavage steps as shown in Fig. 21.

Various mechanisms can be suggested to explain the simultaneous occurrence of cleavage steps and dislocations introduced during cleavage:

1. As discussed by Gilman[29] cleavage steps are produced during cleavage when the cleavage crack intersects screw-dislocations. These screw dislocations may already be present in the crystal or they may be screw dislocations introduced during cleavage ahead of the cleavage crack. An indication that the intersection of dislocations is responsible for the formation of cleavage steps can be seen in Fig. 10.

These dislocations introduced during cleavage take the form of closed loops[40] which are nucleated by the high stresses at the tip of the cleavage crack, and are then bisected by the crack. If the cleavage crack propagates at less than a critical rate, these half-loops may expand to such a size as to remain stable in the crystal. This would require that identical patterns of etch pits should be obtained when chemically etching both sides of the cleavage crack. The fact that this is usually not the case, as shown in Figs. 18 and 20, is that the stresses may not be symmetrical around the tip depending on the method of cleavage and therefore the stresses at only one side of the cleavage crack may be sufficient to expand the half-loops to such a size so that they are stable and do not collapse.

This is also supported by the experimental observation that only one example could be found where a one-to-one correspondence existed between slip lines on the interfaces between surfaces on opposite sides of a cleavage crack and nickel drops. If the dislocation loops nucleated ahead of the cleavage crack grew large enough so that stable half-loops would remain at both sides of the cleavage crack, then a one-to-one correspondence would occur more often.

2. Cleavage steps are also initiated at the start of the cleavage crack,

it being practically impossible to start the crack on one atomic plane only. It has been observed experimentally that most of the higher cleavage steps originate at the point at which cleavage was started. During the propagation of the cleavage crack through the crystal considerable shear will be produced in the vicinity of these cleavage steps. This may slow down the crack to such an extent that it propagates at a rate which permits the loops, nucleated at the tip of the cleavage crack, to expand and to remain as stable half-loops in the crystal, as discussed previously. This is illustrated clearly in Fig. 19 where the high cleavage step is one initiated at the start of cleavage. This slowed the crack down such that the dislocation loops nucleated at the tip grew large enough to be stable as indicated by the presence of etch pits. The crack intersected these dislocation loops and, as discussed above, gave rise to additional cleavage steps indicated by the irregular lines roughly perpendicular to the high cleavage step. The boundary of the band of etch pits indicates the location where the rate of propagation of the cleavage crack changed discontinuously.

3. It may also be possible that even when the rate of propagation of the cleavage crack in the vicinity of cleavage steps is too high for dislocation loops to become stable, the shear stresses at the crack front, due to the propagation of the cleavage steps initiated at the start of cleavage, may be sufficient to expand the dislocation loops nucleated at the tip of the cleavage crack to remain as stable loops in the crystal. This mechanism may explain the occasional row of dislocations which seem to start at a cleavage step as shown in Fig. 21.

4. Some evidence exists which indicates that the grown-in dislocations are responsible for the $\langle 100 \rangle$ arrays of dislocations as more of these arrays seem to occur in platelets cleaved from crystals which were not annealed than

in platelets cleaved from annealed crystals. In addition, as shown in Fig. 21, a row of dislocations seems to be nucleated where a cleavage step intersects a subgrain boundary.

From many observations on etched cleavage faces, it was concluded that most half-loops were introduced by the second mechanism. By the evidence mentioned, some half-loops were also introduced by the third and fourth mechanisms. It was never observed that half-loops were introduced by the first mechanism.

The occurrence of rows of dislocation half-loops is due to the multiplication of a single half-loop. Once a single half-loop has been nucleated it can act as a trigger[18] for further half-loops in the same slip plane. The multiplication of a loop once it has been nucleated is not necessary for the formation of slip sources, as it has been shown experimentally that slip lines occurred on the interface between a nickel drop and a chemically etched platelet of magnesium oxide which did not exhibit any $\langle 100 \rangle$ rows of etch pits. The slip sources then consist of single dislocation half-loops. An example of this may be seen in Figs. 21 and 22, where a slip line goes through two etch pits only.

Washburn, Gorum and Parker[17] also observed these dislocations, introduced during cleavage. However, in their specimens the rows of etch pits which showed up after etching ran along the length of the specimen only. From this it was concluded that these dislocations could not affect the ductile properties as the Burger's vector of these dislocations is oriented perpendicularly to the applied stress.

In the present investigation it was shown that in cleavage approximately an equal number of slip sources were introduced on all slip planes.

Therefore it can be concluded that only those half-loops oriented in the direction of crack propagation can trigger the nucleation of rows of half-loops. The half-loops oriented perpendicularly to the direction of crack propagation do not multiply but can still act as slip sources. The conclusions reached by Washburn, Gorum and Parker[17] should therefore be altered.

K. Slip Source Density

A calculation based on the number of slip lines produced shows that the number of slip sources introduced during cleavage varies from a maximum of approximately fifteen thousand slip sources per $cm.^2$ for a surface with a high density of cleavage steps to no slip sources on a surface without cleavage steps (see Appendix VI)..

The experimental observation that rods, when bent by hand, exhibited varying degrees of ductility before fracture, can be explained by assuming that the more ductile rods had more surface sources than the relatively brittle rods. This is supported by the observation that those rods which possessed a face formed by cutting the crystal with the diamond saw were invariably ductile. That a rough surface treatment leads to introduction of slip sources has been observed by Stokes, Johnston and Li,[18] who introduced dislocations in the surface of polished magnesium oxide rods simply by sprinkling the surface with 46-mesh carborundum powder from a height of three inches. The relative ductility can also be explained if slip took place on one slip system only. This way dislocation pile-up and subsequent crack formation leading to fracture,[19] is avoided.

L. Minimum Size of Stable Dislocation Loop.

A calculation of the minimum size of a closed dislocation loop which can remain in the crystal shows this to be approximately one micron. The

minimum size of a stable dislocation half-loop will probably exceed this figure somewhat. This compares favourably with the average depth of a few microns and the observed distance between etch pits of approximately one and one half microns, assuming that these two etch pits belong to the same loop.

The minimum size of loop is probably a function of temperature and would depend on the relative temperature dependence of dislocation tension and minimum shear stress of dislocation glide. Most of the loops remain stable at 1500°C as they act as slip sources at this temperature. In addition, as shown in Fig. 9, where liquid nickel etched a row of dislocations at 1500°C. they did not have a tendency to move. (For calculation see Appendix VII).

The experimental observation that no more slip is produced at the highest cooling rate than at a lower cooling rate could be because of this minimum size of stable dislocation loop.

M. Depth of Slip Sources.

From the following experimental observations, it can be concluded that the slip sources are located at or just below the cleavage surface:

1. The dislocation half-loops introduced during cleavage were responsible for the slip. These half-loops were observed to extend only a few microns into the surface.

2. No slip lines could be observed on the interface between a nickel drop and a platelet of magnesium oxide which was polished in hot phosphoric acid for about ten minutes. As hot phosphoric acid attacks the surface at a rate of approximately one micron/min.[19] it can be concluded that no slip sources can be found which are more than ten microns below the surface.

3. Additional, but not conclusive, evidence is as follows:

When chemically etching a rod with a nickel drop one can detect two sets of $\langle 110 \rangle$ slip lines and one set of (100) slip lines parallel to the length of the rod. In the bottom face, only (100) slip lines can be seen which are perpendicular to the length of the rod. Recalling that slip with respect to the interface takes place over the four $(110)_{45}$ planes only, one can conclude that the slip lines, as observed on the side and bottom faces of the rod, are lines of intersection of slip planes originating at or in the vicinity of the top surface. This, of course, can also be explained by assuming that the thermal stresses exceed the yield stress in the surface only.

The presence of $\langle 110 \rangle$ slip lines on the side face of the chemically etched rod could lead one to conclude that slip also occurs over $(110)_{90}$ planes, but as a $(110)_{90}$ plane with respect to one cleavage plane is a $(110)_{45}$ plane with respect to a perpendicular cleavage plane, one can still define the slip taking place over $(110)_{45}$ planes only. The difficulty of definition on which plane slip takes place is removed if one defines the slip plane with respect to the surface at which the slip source is located. Slip then takes place on $(110)_{45}$ planes only. The $\langle 110 \rangle$ slip traces in the tension and compression surface of the bent rod, such as in Figs. 18 and 24, are due to slip nucleated at the side surfaces, although with respect to the top surface this would be $(110)_{90}$ slip.

N. Number of Dislocations Produced by Slip Sources.

An estimate can be made of the maximum number of dislocations produced by the slip sources when activated by the thermal stresses. Each time a dislocation on a $(110)_{45}$ plane emerges on the surface, the height of the slip line, as measured perpendicularly to the surface, is increased by a length equal to half the lattice parameter or approximately 2.1×10^{-8} cm. As the height of the step, as measured perpendicularly to the surface, equals its apparent width when viewed perpendicularly to the surface, its height can be

estimated by measuring its width. As shown in Fig. 10, the width is no more than half a millimeter wide at a magnification of 2500x, which makes its height approximately 2×10^{-5}cm. This corresponds to a total number of approximately one thousand dislocations.

It is felt that the slip sources can produce a maximum number of dislocations after which they are rendered inactive. This can be concluded from the experimental observation that on thermal cycling no change in the appearance of the slip lines can be detected. In addition, a platelet with a nickel drop heated to 1800°C did not seem to have any higher slip lines than one cooled from 1500°C. Observations made by Pask[27] also support this view.

Slip sources can be rendered inactive through various mechanisms:

1. This could take place by pile-up of dislocations against subgrain boundaries or against other regions of slip. The combined back-stress of the piled-up dislocations could increase the shear stress required to operate the source to exceed the thermal stresses. Pile-up against subgrain boundaries does not occur in magnesium oxide as shown in Fig. 22.

2. In the case of magnesium oxide the sources activated by the thermal stresses may be destroyed by the deformation it produces. This is because these slip sources are located near the surface. Each time the source produces a dislocation it will have advanced to the surface a distance as measured along the slip plane equal to its Burger's vector. If enough dislocations can be produced the slip source will come out to the surface and will cease to exist.

It is not necessary for the source to move to the surface to be rendered inactive. Assuming the source takes the form of a double-ended

Frank-Read source it will cease to operate when the points at which the dislocation is anchored are within a distance from the surface equal to half the critical length of the source. The critical length of a double-ended Frank-Read source is the distance between the anchoring points below which, at a certain stress level, the source will not operate.

As only half the stress is needed to operate a single-ended Frank-Read source of the same length, the same stress will operate a single-ended source half the length of the double-ended source. Therefore, the source can approach the surface to within a distance equal to half its length.

A calculation of the critical length of a double-ended Frank-Read source, based on a yield-stress of 3.1×10^8 dynes per cm.^{2} at 1500°C, showed it to be approximately one micron. The source will then cease to operate when its anchoring points are within half a micron from the surface.

O. Mechanism of Dislocation Multiplication.

One mechanism by which the dislocation half-loops can act as slip sources is by the formation of jogs in the dislocation loops by either the loops intersecting a grown-in dislocation or by the loops intersecting loops nucleated on other slip planes.

If the loop acquires one jog it can operate as a Frank-Read half-source. If the loop acquires two jogs, it can act as a double-ended Frank-Read source.

If the density of grown-in dislocations is 10^5 per cm.^{2} then a half-loop with a diameter of five microns will, on the average, have intersected 0.01 dislocation. The probability of jog formation does seem rather low. However, it is not necessary for the loop to have acquired jogs when formed.

It can form jogs when undergoing expansion under applied shear stresses. This way the loop may intersect a considerable amount of dislocations which then leads to anchoring.

P. Intrinsic Slip Sources.

In addition to slip sources in the surface introduced during cleavage, evidence exists for the presence of 'intrinsic' slip sources. This can be concluded from the fact that a rod which was polished for ten minutes in hot phosphoric acid to remove all surface sources, exhibited evidence of plastic deformation when bent and subsequently etched as shown in Fig. 23. It is clear that the sources responsible for slip in the polished rod are of a different nature from the surface sources in an 'as cleaved rod', by comparing Fig. 29 with Fig. 30 which shows an area of a plastically deformed rod, which had not been polished. The slip lines in the polished rod appear to be wider than the slip lines in the rod in the 'as cleaved' condition. This suggests that the intrinsic sources, when activated under a shear stress, generate dislocations by a mechanism different from the mechanism by which the surface sources generate dislocations.

It is felt that the faint $\langle 110 \rangle$ lines observed in Fig. 13 may be due to slip caused by the generation of dislocations by the intrinsic sources. It can be concluded, however, that the intrinsic sources contribute very little to the ductility of magnesium oxide crystals, activated by thermal stresses, such as occur under the nickel drop. This could be due to the fact that these thermal stresses may not be high enough to activate the 'intrinsic sources'. This is supported by observations by Stokes, Johnston and Li where it was found that the activation stress for slip in polished magnesium oxide rods was much greater than the stress for slip in rods which contained surface sources.

Q. Chemical Reactions at Interface.

From the experimental observations a hypothesis may be developed for the type of chemical reactions which occurred at the interface. The reaction according to

$$MgO + Ni \leftrightarrows Mg + NiO$$

probably did not take place. First, no evidence for the formation of nickel oxide has been found and second, the nickel oxide is unstable at these temperatures and pressures, as calculated in Appendix VIIIa.

A more probable source for the magnesium is the dissociation of the magnesium oxide into free magnesium and oxygen according to

$$2\ MgO \leftrightarrows 2\ Mg + O_2$$

This dissociation is not impossible, as indicated by a thermodynamic calculation (Appendix VIIIb). In addition, it was experimentally observed that the magnesium oxide is highly volatile.

This magnesium then alloys with the nickel to form the magnesium nickel compound. This results in the removal of the magnesium, which leads to a faster decomposition of the magnesium oxide at the interface. A high enough driving force is present in the form of the heat of formation and the entropy of mixing so that the compound is stable at these temperatures. Fig. 34 shows that the compound exists below 768°C only.

A calculation of the minimum thickness of the interfacial layer such that complete wetting will occur shows this to be 38.4 Å. (See Appendix VIIIc).

The experimental observation of 'etching' of the magnesium oxide by the liquid nickel at the perimeter of the interface is evidence that the decomposition of magnesium oxide occurs preferentially at the perimeter of the interface.

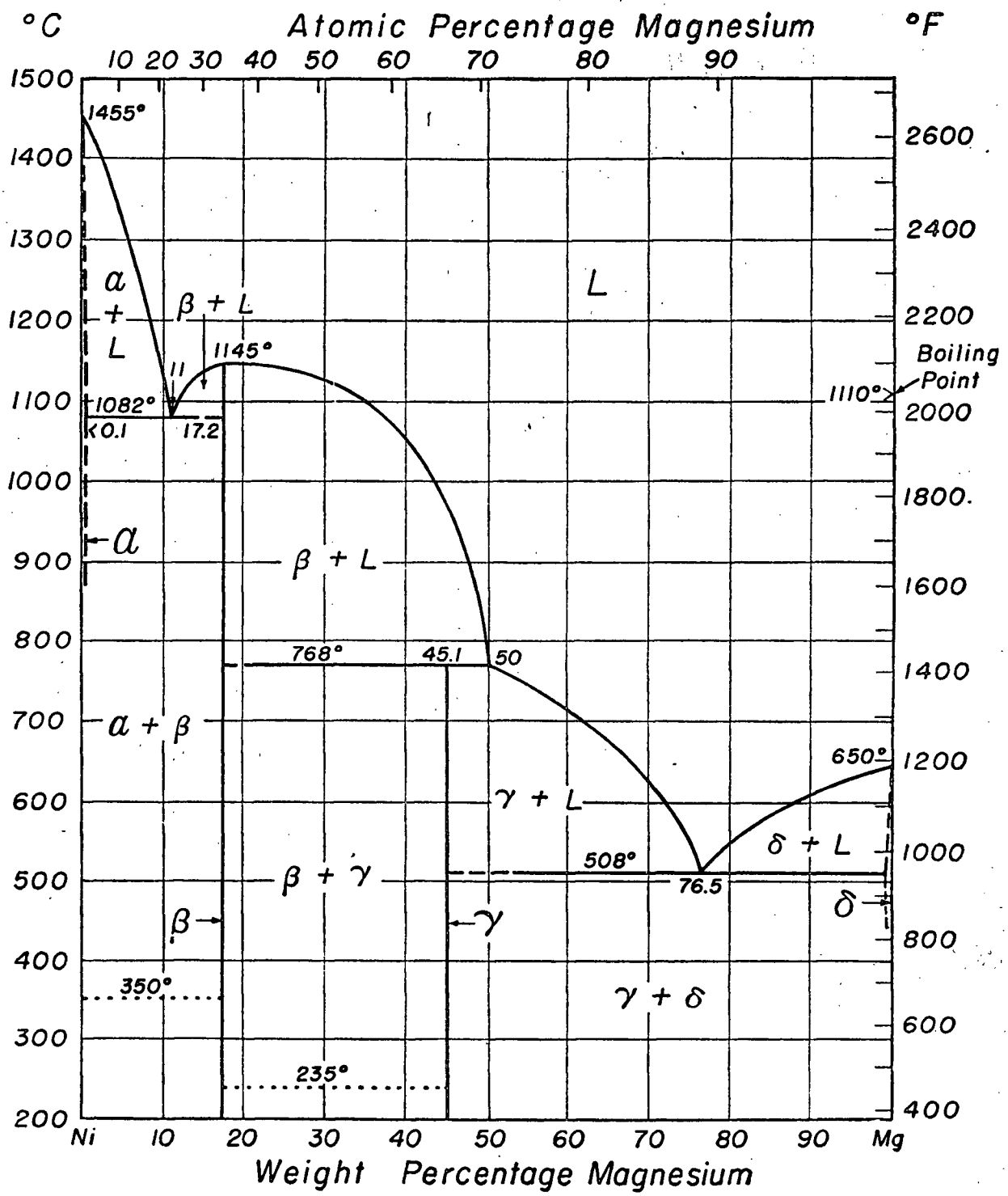

Fig. 34. Nickel-magnesium binary system.

The driving force responsible for the preferential attack at the perimeter of the interface is provided by the equilibrium between the surface- and interfacial tensions. Shown in Figs. 35a and 35b are the configurations of a nickel drop on an etched and unetched magnesium oxide crystal. Replacing

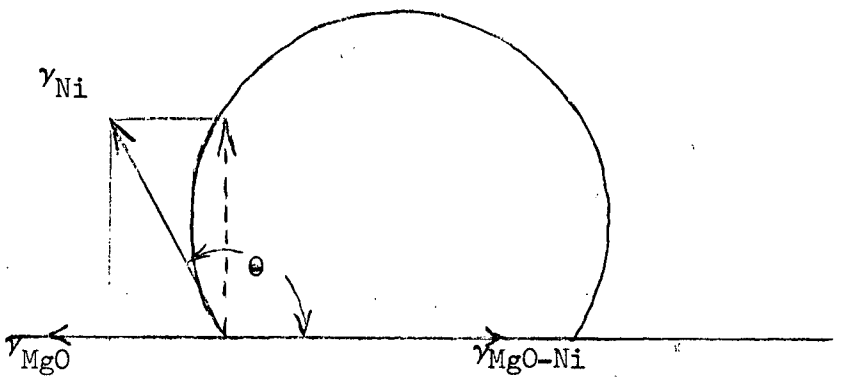

a. Unetched

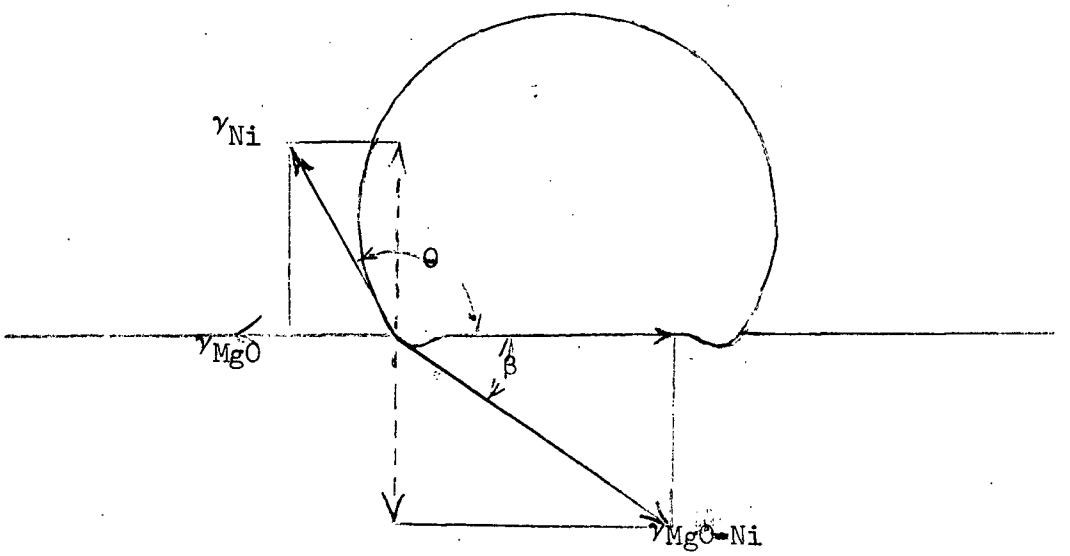

b. Etched

Fig. 35. Surface tensions equilibria.

the interfacial energies per unit area by interfacial tensions per unit length and resolving these forces in the plane of the figure results in the equilibria shown above. β is the angle through which the interfacial tension

between the magnesium oxde and the nickel is rotated due to the appearance of the groove at the perimeter.

The driving force for the reaction which leads to the groove formation results from the fact that when a groove is formed all the forces are in equilibrium. On a flat surface this is the case for the horizontal components only.

The equilibrium of the forces in the horizontal plane is given by $\gamma_{MgO} - \gamma_{Ni} \cos \Theta = \gamma_{MgO-Ni} \cos \beta$. During evaporation of the drop the term $\gamma_{Ni} \cos \Theta$ continuously decreases. This upsets the equilibrium. The drop will contract catastrophically when the imbalance of the equilibrium has reached such a value that the drop can reattain the equilibrium configuration it will have on a flat surface. The cycle repeats itself when a new groove is formed.

It is this groove formation which is responsible for the observed hysteresis of wetting. It can be concluded that little or no value can be attached to the wetting angles reported in Table III. Most of these will represent a non-equilibrium wetting angle. Only those angles which are measured immediately after a contraction of the drop would be an indication of the wettability of the magnesium oxide. It is clear that the method of studying metal-ceramic interaction by means of wettability experiments does not lend itself to the system magnesium oxide-nickel.

R. Etching of Dislocations by Liquid Nickel

Liquid nickel also etches magnesium oxide preferentially at dislocations and subgrain boundaries. The driving force for this is the state of higher energy of the lattice at dislocations and subgrain boundaries. This leads to a faster decomposition of the magnesium oxide, which results in etch pit formation.

S. Diffusion of Nickel into Magnesium Oxide.

The diffusion of nickel into magnesium oxide single crystals seems to occur mainly by diffusion along dislocations. This is indicated by a much slower rate of etching of old dislocations compared with fresh dislocations. These fresh dislocations were introduced at room temperature after diffusion took place. If the nickel were distributed uniformly through the magnesium oxide crystal, the etching rate for all dislocations would be approximately equal.

Additional evidence that diffusion occurs along dislocations is that greater amounts of nickel are present in those crystals which were plastically deformed. The actual relative amounts of diffused nickel were not determined. Removal of the drops by shear removes part of the diffused nickel. Removal of the drop by melting, may introduce extra dislocations. Also, some of the nickel may diffuse out as indicated by the experimental observation that little nickel could be found in those crystals from which the drop was removed by evaporation. Although in the preparation of the specimens part of the nickel was removed, it is felt that sufficient evidence exists to conclude that bulk-diffusion takes place by diffusion along dislocations.

Close analysis of the results obtained by Turnbull[26] indicate that those dislocations introduced in the surface during cleavage also affect the diffusion of nickel into magnesium oxide.

During evaporation of the drop between contractions, equilibrium could be preserved if interfacial tension near the perimeter could be decreased. This could take place by extra diffusion of the nickel into the magnesium oxide. The interfacial tension between a nickel rich magnesium oxide and nickel will be lower than the interfacial tension between pure

magnesium oxide and nickel. It is felt that this mechanism is responsible for the fact that little or no chemical etching occurred near the perimeter of the interface as shown in Fig. 27.

T. Strength of Bond.

The bond strength between magnesium oxide and nickel exceeds the fracture stress of the magnesium oxide. On removal of the nickel drop from the magnesium oxide, fracture occurs through the magnesium oxide rather than through the interface.

The formation of the magnesium-nickel compound at the interface is necessary for the formation of the strong bond. This is indicated by the experimental observation that a drop held at a temperature just above its melting point for approximately ten seconds does not adhere as well as those held at 1500°C for ten minutes. The amount of compound formed in ten seconds will be less than the amount formed in ten minutes.

The presence of nickel oxide at the interface has a detrimental effect on the bond strength. When removing a nickel drop, which initially contained 2% nickel oxide, fracture occurred at the interface between the drop and magnesium oxide.

Bond strength between magnesium oxide and metals, in general, will be affected by the formation of gas occlusions at the interface. It was observed that on the interfaces between magnesium oxide and metals such as silver, copper, aluminum and tin, many gas occlusions formed. Moore and Thornton[8] made the same observation for the system gold-silica. They attributed the formation of gas occlusions to the presence of traces of oxygen in the vacuum used.

V. CONCLUSIONS

A. Ductility

The magnesium oxide under the nickel drop is deformed by thermal stresses which are developed during cooling. Slip takes place on the four $\langle 110 \rangle$ slip planes inclined at 45° to the cleavage plane. The slip does not seem to be affected by the presence of subgrain boundaries.

The amount of plastic deformation is a function of the rate of cooling. More deformation occurs at greater cooling rates. At the maximum cooling rates possible no more slip is produced than at a lower cooling rate. At less than the maximum cooling rate all the slip sources present are activated.

Because of the plastic deformation, a bending moment exists upon cooling. As the deformation occurred by compression, the region of the magnesium oxide directly under the nickel drop will be under tension when cooled to room temperature.

Heating metal drops, such as aluminum, copper and silver to a temperature 50°C above their respective melting points, does not give rise to plastic deformation when cooled, due to lower thermal stresses and a higher yield point of the magnesium oxide. When a silver drop is heated to 1400°C, thermal stresses on cooling are high enough to give plastic deformation.

The slip sources activated by these thermal stresses are introduced in the surface of the magnesium oxide during cleavage. The average depth of these sources is of the order of a few microns. No slip sources activated by these thermal stresses exist at a depth exceeding ten microns.

The introduction of slip sources in the surface by cleavage is

associated with the formation of cleavage steps. No slip sources exist in surfaces which do not have cleavage steps.

The slip source density varies from a maximum of fifteen thousand sources per $cm.^2$ for a surface with a high density of cleavage steps to no slip sources for a surface without cleavage steps.

The slip sources introduced in the surface during cleavage take the form of dislocation half-loops. The formation of cleavage steps during the propagation of the cleavage crack slows down the rate of propagation of the crack or gives rise to enough shear such that dislocation loops, nucleated ahead of the cleavage crack, grow to a size such that they can remain as stable half-loops in the surface when cut by the passing cleavage crack.

The calculated minimum size of stable dislocation loop agrees well with the observed value of approximately one micron.

Etching of these cleavage faces results in the production of etch pits at these dislocation loops. Rows of etch pits are due to the multiplication of dislocation loops located on slip planes oriented parallel to the direction of propagation of the cleavage crack. Continued etching removes the half-loops from the crystal.

The multiplication of the half-loops is probably due to formation of jogs, which then anchor the dislocation. Under an applied shear stress the half-loops can then multiply and do not move out of the crystal.

The number of dislocations produced by a slip source is approximately one thousand. The slip source stops operating due to dislocation pile-ups or by moving to the surface due to the deformation it causes.

This method of inducing thermal stresses in cleavage surfaces lends itself very well to studying the behaviour of surface slip sources in magnesium oxide and may well be applicable to other materials.

B. Chemical Reactions and Diffusion.

The bonding mechanism between nickel and single crystals of magnesium oxide consists of the formation of a magnesium nickel (Mg_2Ni) compound as indicated by X-ray analysis of the interfacial material. The bonding force between the nickel and magnesium oxide exceeds the fracture stress of magnesium oxide, shown by the fact that removal of the nickel drop leads to fracture through the magnesium oxide.

The wettability results showed a large hysteresis of wetting. This hysteresis of wetting is due to the formation of a 'groove' at the perimeter of the interface between the nickel and magnesium oxide. For this reason, the method of studying metal-ceramic interactions by means of wettability measurements can not be used in the system nickel-magnesium oxide.

Bulk-diffusion of nickel into single crystals of magnesium oxide seems to take place by diffusion along dislocations. This is indicated by the relative amounts of nickel in deformed and undeformed crystals.

RECOMMENDATIONS FOR FUTURE WORK

It is felt that by using this technique no further understanding can be gained of the ductile properties of magnesium oxide. However, certain observations were made which may warrant further investigation.

Quantitative measurement of the diffusion of metals into magnesium oxide as a function of dislocation content may indicate to what extent the presence of dislocations is responsible for bulk diffusion. Magnesium oxide could lend itself very well for this as it might not recover from any plastic deformation introduced even if these tests were carried out at fairly high temperatures.

More understanding can be gained of the size, distribution and nature of the dislocation loops introduced during cleavage. The X-ray technique developed by Berg and Barrett might be applicable to this problem.

A study of the wettability of magnesium oxide by other metals or alloys can also be of interest. The variations in the wetting may be followed by motion film techniques and may throw more light on the mechanisms of the hysteresis of wetting.

During the X-ray fluorescent qualitative analysis of the magnesium oxide, it was noticed that single crystals would turn a wine-red, whereas powdered magnesium oxide would remain colorless. It could be of interest to investigate this phenomenon, although this could carry over into the field of solid state physics.

APPENDIX I

X-ray Diffraction Data from Nickel-Magnesium Oxide Interface.

Photographic prints of X-ray powder patterns of the interfacial material and pure magnesium oxide are shown in Fig. 36.

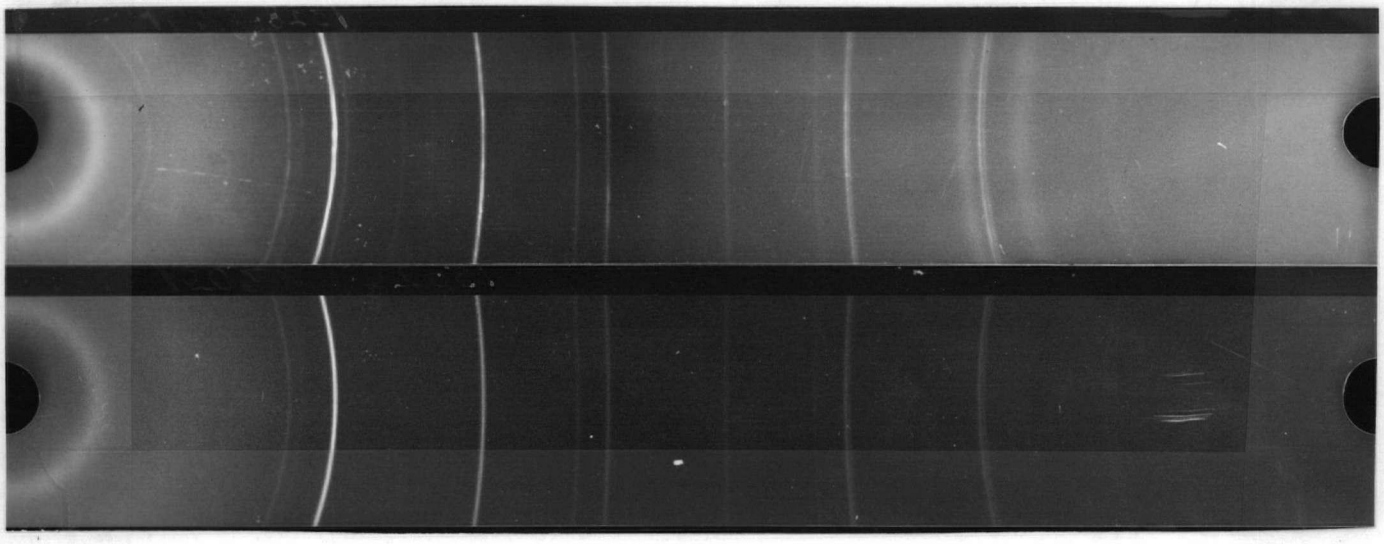

Fig. 36. X-ray powder patterns Nos. 1502 and 1528. (Top - interfacial material, bottom - pure magnesium oxide).

The observed X-ray data for the interfacial material and the material present as identified from the A.S.T.M. Card Index are shown in Table IV. The reported d-values for the materials present are shown in Figs. 37, 38 and 39. Comparing the data from the A.S.T.M. cards for magnesium oxide, magnesium nickel compound and magnesium hydroxide, one can conclude that all these three materials are present. The lines which could be responsible for more than one material could be partially due to the presence of Ni as these two lines are the two strongest lines reported for nickel, as shown in Fig. 41. The presence of magnesium hydroxide might be explained by magnesium oxide reacting with the moisture from the air or perhaps with traces of water in the grease used in the preparation of the specimen for X-ray analysis. From the relative intensities of the lines, one can conclude that the magnesium

TABLE IV.

Data from Film No. 1528

Line	I/I_o	d	Material
1	15	4.7612	$Mg(OH)_2$
2	10	4.4357	Mg_2Ni
3	1	3.1120	Mg_2Ni
4	20	2.4351	MgO
5	5	2.3351	$Mg(OH)_2$
6	<1	2.2510	Mg_2Ni
7	100	2.1091	MgO
8	10	2.0359	Mg_2Ni, Ni
9	2	1.7653	Mg_2Ni, Ni, $Mg(OH)_2$
10	1	1.6488	Mg_2Ni
11	50	1.4999	MgO
12	10	1.2696	MgO
13	15	1.2169	MgO
14	1	1.1315	Mg_2Ni
15	5	1.0496	MgO
16	5	.96382	MgO
17	10	.93956	MgO
18	10	.85786	MgO
19	5	.81007	MgO

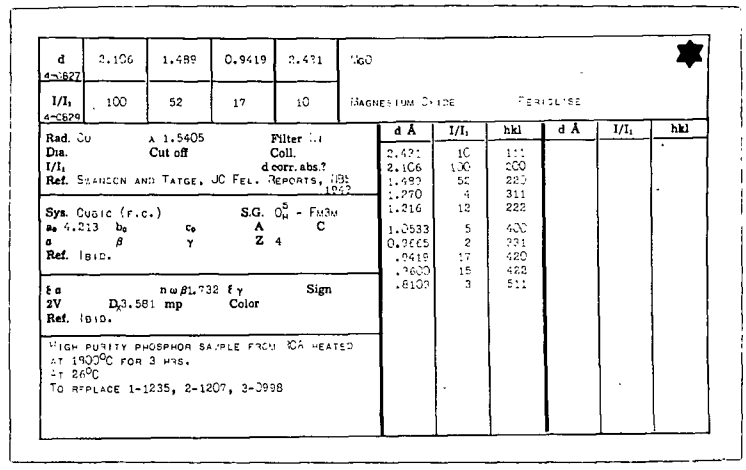

d	2.106	1.489	0.9419	2.431	MgO
4-0827					
I/I$_1$	100	52	17	10	MAGNESIUM OXIDE PERICLASE
4-0829					

Rad. Cu λ 1.5405 Filter Ni
Dia. Cut off Coll.
I/I$_1$ d corr. abs.?
Ref. SWANSON AND TATGE, JC FEL. REPORTS, (B)1, 1947

Sys. CUBIC (F.c.) S.G. O_h^5 - Fm3m
a_o 4.213 b_o c_o A C
α β γ Z 4
Ref. IBID.

ε α n ω β1.732 ε γ Sign
2V D_x3.581 mp Color
Ref. IBID.

HIGH PURITY PHOSPHOR SAMPLE FROM NBS HEATED AT 1900°C FOR 3 HRS.
AT 26°C
TO REPLACE 1-1235, 2-1207, 3-0998

d Å	I/I$_1$	hkl	d Å	I/I$_1$	hkl
2.431	10	111			
2.106	100	200			
1.489	52	220			
1.270	4	311			
1.216	12	222			
1.0533	5	400			
0.9665	2	331			
.9418	17	420			
.8600	15	422			
.8103	3	511			

Fig. 37. A.S.T.M. Card No. 4.0829 for magnesium oxide.

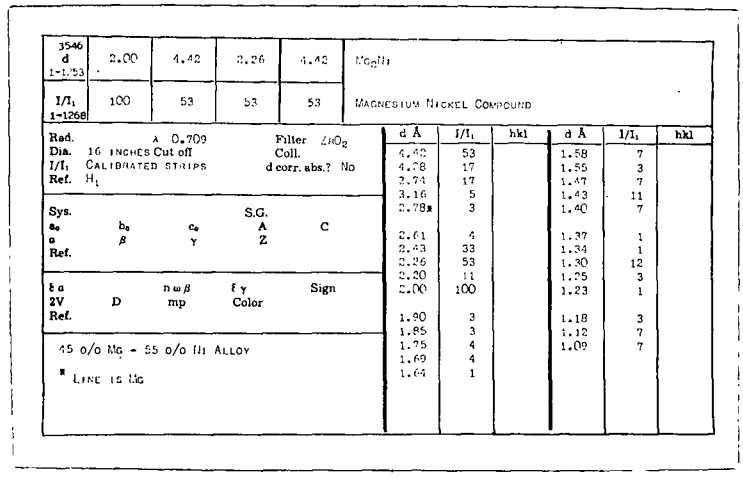

3546 d	2.00	4.42	2.26	4.42	Mg_2Ni
1-1153					
I/I$_1$	100	53	53	53	MAGNESIUM NICKEL COMPOUND
1-1268					

Rad. λ 0.709 Filter ZrO_2
Dia. 16 INCHES Cut off Coll.
I/I$_1$ CALIBRATED STRIPS d corr. abs.? No
Ref. H$_1$

Sys. S.G.
a_o b_o c_o A C
α β γ Z
Ref.

ε α n ω β ε γ Sign
2V D mp Color
Ref.

45 o/o Mg - 55 o/o Ni ALLOY

* LINE IS Mg

d Å	I/I$_1$	hkl	d Å	I/I$_1$	hkl
4.42	53		1.58	7	
4.28	17		1.55	3	
3.74	17		1.47	7	
3.16	5		1.43	11	
2.78*	3		1.40	7	
2.61	4		1.37	1	
2.43	33		1.34	1	
2.26	53		1.30	12	
2.20	11		1.25	3	
2.00	100		1.23	1	
1.90	3		1.18	3	
1.85	3		1.12	7	
1.75	4		1.09	7	
1.69	4				
1.64	1				

Fig. 38. A.S.T.M. Card No. 1.1268 for magnesium nickel compound (Mg_2Ni).

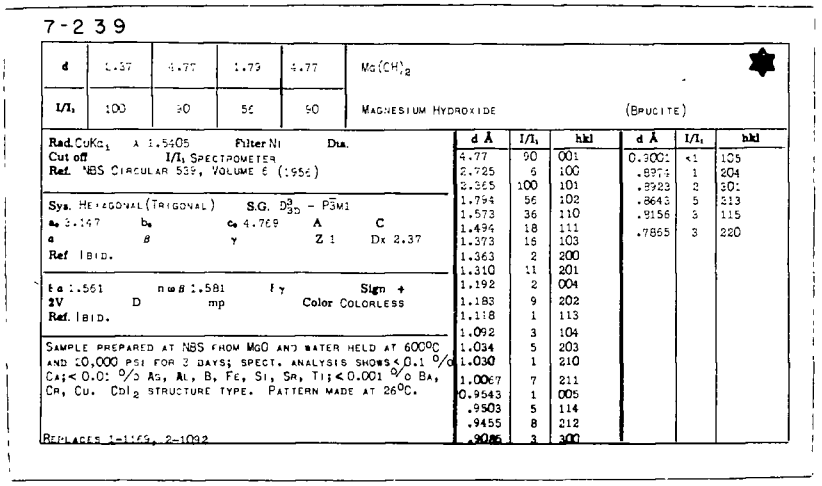

7-239

d	2.37	4.77	1.79	4.77	$Mg(OH)_2$
I/I₁	100	90	56	90	MAGNESIUM HYDROXIDE (BRUCITE)

Rad. $CuK\alpha_1$ λ 1.5405 Filter Ni Dia.
Cut off I/I₁ SPECTROMETER
Ref. NBS CIRCULAR 539, VOLUME 6 (1956)

Sys. HEXAGONAL (TRIGONAL) S.G. $D_{3d}^3 - P\bar{3}M1$
a_o 3.147 b_o c_o 4.769 A C
α β γ Z 1 Dx 2.37
Ref IBID.

ε α 1.561 nω β 1.581 ε γ Sign +
2V D mp Color COLORLESS
Ref. IBID.

SAMPLE PREPARED AT NBS FROM MgO AND WATER HELD AT 600°C AND 10,000 PSI FOR 3 DAYS; SPECT. ANALYSIS SHOWS < 0.1 % Ca; < 0.01 % Ag, Al, B, Fe, Si, Sn, Ti; < 0.001 % Ba, Cr, Cu. CdI_2 STRUCTURE TYPE. PATTERN MADE AT 26°C.

REPLACES 1-1169, 2-1092

d Å	I/I₁	hkl	d Å	I/I₁	hkl
4.77	90	001	0.9003	<1	105
2.725	6	100	.8973	1	204
2.365	100	101	.8928	2	301
1.794	56	102	.8643	5	213
1.573	36	110	.8156	3	115
1.496	18	111	.7865	3	220
1.373	16	103			
1.363	2	200			
1.310	11	201			
1.192	2	004			
1.183	9	202			
1.118	1	113			
1.092	3	104			
1.034	5	203			
1.030	1	210			
1.0067	7	211			
0.9543	1	005			
.9503	5	114			
.9455	8	212			
.9085	3	300			

Fig. 39. A.S.T.M. Card No. 7.239 for magnesium hydroxide.

nickel compound existed at the interface or within the magnesium oxide. It did not exist within the metal drop as this would require that the whole drop consisted of the compound. This could be the case if the attack of the magnesium oxide was much greater than could be detected metallographically. From the relative line intensity it can be concluded that only a small amount of nickel was removed from the nickel drop in the preparation of the powder specimen. As the line intensities of the nickel-magnesium compound are at least as great as those which could be due to nickel, it can be concluded that the compound existed at the interface. Also it can be concluded that nickel oxide and magnesium exist in quantities not large enough to be detected by X-ray analysis.

Any nickel oxide that formed could possibly exist in the form of nickel oxide-magnesium oxide solid solution. However, as these lines have approximately the same d-values as magnesium oxide, any evidence for the existence of the solid solution is completely obscured by the presence of the magnesium oxide. Comparison of the relative line intensities of magnesium oxide and nickel oxide-magnesium oxide (A.S.T.M. Card No. 3.0990) shows the lines, at least for the greatest part, to be due to magnesium oxide.

APPENDIX II

X-ray Diffraction Data from Interface Between Magnesium Oxide and Nickel + 2% NiO.

A photographic print of the X-ray powder pattern of the interfacial material between magnesium oxide and nickel + 2% nickel oxide is shown in Fig. 40. The observed X-ray data for the interfacial material and the

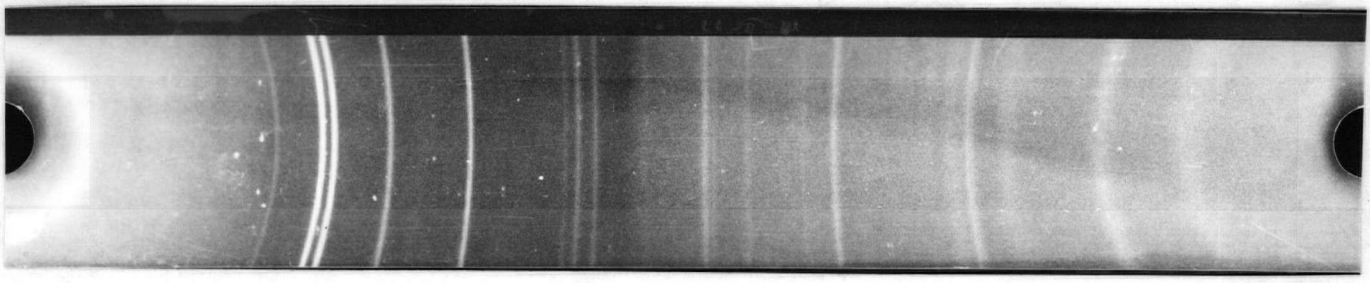

Fig. 40. X-ray powder pattern No. 1530 of interfacial material between magnesium oxide and nickel + 2% nickel oxide.

material present, as identified from the A.S.T.M. Card Index, are shown in Table V. The A.S.T.M. cards for nickel and nickel oxide are shown in Figs. 41 and 42.

It can be concluded that the material at the interface consists of nickel oxide and nickel only. The presence of the nickel oxide-water compound can be explained, as for the presence of magnesium hydroxide (see Appendix I), by assuming that the nickel oxide reacts with the water in the air or with water in the grease used in the preparation of the powder specimen. The lack of evidence for the existence of magnesium oxide in the interfacial material supports the experimental observation that fracture occurred at the interface rather than through the magnesium oxide, as happens with drops composed of pure nickel. From the relative line intensities of nickel and nickel oxide can be concluded that the nickel oxide, in addition to segregating

TABLE V

Data from Film No. 1530

Line	I/I_o	d	Material
1	10	2.4287	NiO
2	5	2.3374	$NiO.H_2O$
3	100	2.1044	NiO
4	100	2.0351	Ni
5	30	1.7602	Ni
6	35	1.4890	NiO
7	5	1.2621	NiO
8	10	1.2455	Ni
9	8	1.2161	NiO
10	5	1.0596	Ni
11	2	1.0505	NiO
12	1	1.0305	$NiO.H_2O$
13	5	1.0146	Ni
14	1	.96881	NiO
15	5	.95196	NiO
16	5	.85815	NiO
17	5	.80718	Ni
18	5	.78693	Ni

d 4-0854	2.034	1.762	1.246	2.034	Ni
I/I$_1$ 4-0850	100	42	21	100	NICKEL

Rad. Cu λ 1.5405 Filter Ni
Dia. Cut off Coll.
I/I$_1$ d corr. abs.?
Ref. SWANSON AND TATGE, JC FEL. REPORTS, NBS 1951

Sys. CUBIC (F.c.) S.G. O_h^5 - Fm3m
a_o 3.5238 b_o c_o A C
α β γ Z 4
Ref. IBID.

δ α n ω β ε γ Sign
2V D_x 8.907 mp Color
Ref.

SPECTROGRAPHIC ANALYSIS SHOWS <0.01% EACH OF Mg, Si AND Ca.
AT 26°C
TO REPLACE 1-1258, 1-1260, 1-1266, 1-1272, 3-1043, 3-1051

d Å	I/I$_1$	hkl	d Å	I/I$_1$	hkl
2.034	100	111			
1.762	42	200			
1.246	21	220			
1.0624	20	311			
1.0172	7	222			
0.9810	4	400			
.8044	14	331			
.7880	15	420			

Fig. 41. A.S.T.M. Card No. 4.0850 for nickel.

d 4-0838	2.088	2.410	1.476	2.410	NiO
I/I$_1$ 4-0835	100	91	57	91	NICKEL OXIDE BUNSENITE

Rad. Cu λ 1.5405 Filter Ni
Dia. Cut off Coll.
I/I$_1$ G-M COUNTER - d corr. abs.?
Ref. SWANSON AND TATGE, JC FEL. REPORTS, NBS 1950

Sys. CUBIC S.G. O_h^5 - Fm3m
a_o 4.1769 b_o c_o A C
α β γ Z
Ref. IBID.

δ α n ω β 2.73 ε γ Sign
2V D_x 6.806 mp (Li) Color
Ref. IBID.

SPEC. ANAL. SHOWS FAINT TRACES OF Mg, Si, AND Ca.
AT 26°C
TO REPLACE 1-1239, 2-1216, AND 3-1287

d Å	I/I$_1$	hkl	d Å	I/I$_1$	hkl
2.410	91	111			
2.088	100	200			
1.476	57	220			
1.259	16	311			
1.206	13	222			
1.0441	8	400			
0.9582	7	331			
.9338	21	420			
.8527	17	422			
.8040	7	511			

Fig. 42. A.S.T.M. Card No. 4.0835 for nickel oxide.

at the outside of the nickel drop (see Experimental Observations) also segregates at the interface between the nickel drop and the magnesium oxide.

APPENDIX III

Calculation of Wetting Angle from Drop Dimensions

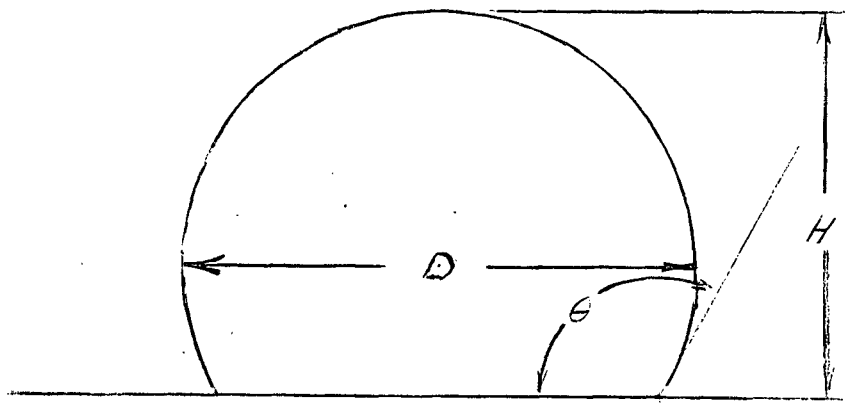

Fig. 43. Drop with necessary dimensions to calculate wetting angle.

The relation between diameter D, height H, and wetting angle θ (see Fig. 43), on the assumption that the drop is spherical, is

$$\cos \theta = \frac{D - 2H}{D}$$

Taking as an example the calculation of the wetting angle of high purity Ni on the 'as cleaved' magnesium oxide 20 minutes after melting, where the following measurements were made:

D = 2.091 inches and

H = 1.290 inches

substitution of these values gives: $\cos \theta = -.229$

from which $\theta = 103.2$

The accuracy by which the wetting angle can be determined by this method is ±2°.

APPENDIX IV

Calculation of Stresses at the Interface between Magnesium Oxide and Nickel Drop Resulting from the Differences in Thermal Expansion.

The difference in thermal expansion per centimeter of interface equals $(\alpha_1 - \alpha_2)\Delta T$,

where α_1 is the coefficient of linear expansion for magnesium oxide[32] and measured to be 13.5×10^{-6} per °C.

α_2 is the coefficient of linear expansion for nickel[33] and equals 13.46×10^{-6} per °C. and

ΔT is the temperature range in °C. through which the specimen was cooled.

On cooling the nickel will be in compression because of its lower coefficient of expansion and the magnesium oxide will be in tension therefore the strains in these materials will be of opposite sign. Therefore the difference in thermal expansions will be equal to the sum of the elastic strains (neglecting bending) in each material. This gives,

$$(\alpha_1 - \alpha_2)\Delta T = \sigma \left\{ \frac{(1 - v)}{E_1} + \frac{(1 - v)}{E_2} \right\}$$

where E_1 is Young's modulus of magnesium oxide[24] and equal to 1.72×10^{12} dynes per cm.^{2}

E_2 is Young's modulus of nickel[34] and equals 2.07×10^{12} dynes per cm.^{2}

σ is the resulting stress at the interface, and

v is Poisson's ratio, here assumed to be equal to .35.

Rearranging gives: $$\sigma = \frac{E_1 E_2 (\alpha_1 - \alpha_2)\Delta T}{(E_1 + E_2)(1 - v)}$$

which gives, upon substitution of the appropriate values,

$$\sigma = 5.78 \times 10^4 \Delta T \text{ dynes per cm.}^2$$

The resolved shear stress on the slip planes then becomes

$$\sigma = 2.89 \times 10^4 \Delta T \text{ dynes per cm.}^2$$

The resolved yield stress[19] at room temperature is approximately 6.90×10^8 dynes per cm.^{2} Therefore the temperature interval through which the specimen must be cooled for the stresses at the interface to exceed the yield stress is where

$$2.89 \times 10^4 \Delta T = 6.90 \times 10^8$$

or

$$\Delta T = \frac{6.90 \times 10^8}{2.89 \times 10^4} = 2.39 \times 10^4 \text{ °C.}$$

As the temperature interval through which the specimen is cooled is approximately 1.4×10^3°C. or only about 6% of the interval required for plastic deformation, it can be concluded that the differences in thermal expansion can not cause plastic deformation.

The accuracy of this calculation is of course dependent on the accuracy by which the coefficients of expansion could be determined. The coefficient of linear expansion for nickel can be assumed to be accurate. The value selected for magnesium oxide was considered to be the most reliable one. Other values reported for the coefficient of linear thermal expansion are 133×10^{-6} per[41] °C. and 13.3×10^{-6} per[14] °C. Calculations based on these values also show that plastic deformation could not have taken place by the differences in contraction on cooling.

APPENDIX V

Calculation of Thermal Stresses at the Interface between the Nickel Drop and the Magnesium Oxide Resulting from Temperature Differences on Cooling.

In principle one can calculate the thermal stresses that occur on cooling by solving the partial differential equation for heat flow to obtain equations for the temperature distribution as a function of time. From these equations the thermal stresses can then be calculated. However, in order to be able to solve the partial differential equation for heat flow, one requires a detailed knowledge of the boundary conditions. It is experimentally impossible to determine these. Even an approximation cannot be made, because of the of the fast response of the temperature of the susceptor to power input. However, an estimation of the thermal stresses can be made. Various models and temperature distributions can be assumed, such as a thin circular disc with a temperature distribution or a body with a higher temperature than its surroundings, but constrained to expand.

The radial and angular stresses for a thin circular disc of radius b with a temperature distribution symmetrical about the center, as given by Timoshenko and Goodier[35] are

$$\sigma_r = \alpha E\left(\frac{1}{b^2}\int_0^b \Delta T r dr - \frac{1}{r^2}\int_0^r \Delta T r dr\right)$$

$$\sigma_\theta = \alpha E\left(-\Delta T + \frac{1}{b^2}\int_0^b \Delta T r dr + \frac{1}{r^2}\int_0^r \Delta T r dr\right)$$

where α is the coefficient of linear expansion

E is Young's modulus

ΔT is the temperature difference between the center of the plate and the perimeter.

r is the distance from the center to the region under consideration.

Assuming a parabolic temperature dependence gives for the temperature distribution

$$T(r) = \Delta T \frac{r^2}{b^2}$$

Substitution of this into the equation for the stresses andintegration gives

$$\sigma_r = \alpha E \Delta T \left(\frac{1}{4} - \frac{r^2}{4b^2} \right) \quad \text{and}$$

$$\sigma_\theta = \alpha E \Delta T \left(\frac{-3}{4} + \frac{r^2}{4b^2} \right)$$

which gives for

$r = 0$ $\quad \sigma_r = \frac{\alpha E \Delta T}{4}$,

$\sigma_\theta = -\frac{3}{4} \alpha E \Delta T$ and for

$r = b$ $\quad \sigma_r = 0$

$\sigma_\theta = -\frac{1}{2} \alpha E \Delta T$

Substituting the values,

$\alpha = 13.5 \times 10^{-6}$ per °C.

and $E = 1.72 \times 10^{12}$ dynes per cm.^{2}

gives for $r = 0$

$\sigma_r = 5.84 \Delta T \times 10^6$ dynes per cm.^{2}

$\sigma_\theta = -17.5 \Delta T \times 10^6$ dynes per cm.^{2}

and at $r = b$

$\sigma_\theta = -11.7 \Delta T \times 10^6$ dynes per cm.^{2}

the corresponding resolved shear stresses at the slip planes will be for

r = 0,

$$\sigma_r = 2.92 \Delta T \times 10^6 \text{ dynes per cm.}^2$$

$$\sigma_\theta = -8.75 \Delta T \times 10^6 \text{ dynes per cm.}^2$$

and for r = b

$$\sigma_\theta = -5.85 \ T \times 10^6 \text{ dynes per cm.}^2$$

The resolved yield stress has been measured to be approximately 3.1×10^8 dynes per cm.^2, therefore plastic deformation will occur at r = 0 when

$$\Delta T = \frac{3.1 \times 10^8}{8.75 \times 10^6}$$

$$= 35.4 \ ^\circ C.$$

and r = b when

$$\Delta T = \frac{3.1 \times 10^8}{5.85 \times 10^6}$$

$$= 53^\circ C.$$

Another more simple calculation is based on the stress necessary to constrain a body from expanding under increase of temperature. In this case the thermal expansion equals the elastic strain due to the applied stress. This gives

$$\alpha \Delta T = \frac{\sigma}{E}$$

where ΔT is the rise in temperature of the body. Rearranging gives

$$\sigma = \alpha E \Delta T$$

$$= 13.5 \times 10^{-6} \times 1.72 \times 10^{12} \Delta T \text{ dynes per cm.}^2$$

$$= 23.2 \times 10^6 \ \Delta T \text{ dynes per cm.}^2$$

The resolved shear stress on the slip planes is then

$$= 11.6 \times 10^6 \ \Delta T \text{ dynes per cm.}^2$$

The temperature rise for the shear stress at 1500°C to be equal to the yield stress

$$\Delta T = \frac{3.1 \times 10^8}{11.6 \times 10^6} = 26.7 \text{ °C.}$$

Assuming that these calculations are applicable to the conditions at the interface between the nickel drop and the magnesium oxide, one can conclude that a temperature difference between the center of the interface and the perimeter of approximately 35°C can produce stresses which will exceed the yield stress. From the second calculation it can be concluded that a mean temperature difference between the region under the drop and the region outside the drop of approximately 25 to 30°C. will also cause plastic deformation. Temperature differences such as these are well within the limits of those expected. Observation of the furnace and specimen when cooling shows that the susceptor will be at a temperature where it does not emit visible radiation in less than thirty seconds. The nickel drop, however, will remain red hot for at least two or three minutes. From this it can be concluded that the areas of the magnesium oxide, not covered by the nickel drop, can emit radiation to a virtually cold body, whereas the area under the drop cannot. It is felt that temperature differences of the order of 100°C. are not impossible.

APPENDIX VI

Calculation of Density of Slip Sources Introduced During Cleavage.

This calculation is based on the following assumptions:

1. each slip line is caused by the presence of one source.

2. all sources under the nickel drop are activated.

3. no slip is produced by sources outside the area of the surface covered by the nickel drop.

4. there is an equal number of sources that give rise to slip lines in one [100] direction as in the perpendicular direction.

5. all the sources produce sufficient slip to be detected by optical means.

6. all the slip lines are continuous from one side of the interface to the other.

Fig. 8 represents an area in the center on the interface between a nickel drop and magnesium oxide platelet at a magnification of 250x. The width of the figure is 10 cm. The diameter of the interface has been measured to be .21 cm. The number of vertical slip lines across the width of the picture, counting from left to right, is approximately 50. These 50 slip lines were produced by slip sources in an area equal to

$$\frac{10}{250} \times .21 \text{ cm.}^2 = 8.4 \times 10^{-3} \text{ cm.}^2$$

As many slip sources are introduced during cleavage for slip in one direction as for slip in its perpendicular direction. Therefore in this area of 8.4×10^{-3} cm.^{2} 100 slip sources are introduced. This gives a slip source density of

$$\frac{100}{8.4 \times 10^{-3}} \approx 12{,}000 \text{ slip sources per cm.}^2$$

Calculations based on the same assumptions for the slip source density of an interface with a high cleavage step density, gave a density of approximately 15,000 slip sources per $cm.^2$.

The assumptions on which these calculations are based are valid in so far that it is reasonable to assume that each slip line is caused by one slip source only. However, it may not be valid to assume that all the sources under the nickel drop are activated as the thermal stresses will be a function of position and may not be high enough in some areas to activate the slip sources. However, the experimental observation that the highest cooling rate did not give rise to more slip lines than a lower cooling rate would indicate that all the sources were activated.

The third, fourth and sixth assumptions are supported by actual experimental observation. However, the assumption that all slip sources produce enough slip to be detected, is not valid. The lowest slip line that may be detected is of the order of 30 Å high,[29] which corresponds to a total production of about fifteen dislocations. The actual plastic deformation amounts to very little. Therefore from the point of view of amount of deformation produced, it seems reasonable to base a calculation of slip source density only on those slip lines which can be detected optically.

APPENDIX VII

Calculation of Minimum Size of Stable Dislocation Loop.

This calculation is based on the assumption that the force which anchors the dislocation loop is the minimum shear stress for dislocation glide. The force which tends to contract the dislocation loop arises from the tension of the dislocation line. By equating these forces and assuming that the loop is circular gives the size of the smallest loop stable in the crystal.

The tension of a dislocation line as given by Cottrell[40]

$$T \simeq 0.5 \mu b^2$$

where T is the tension of the dislocation

μ is the shear modulus

b is the length of the Burger's vector.

The shear modulus can be calculated from

$$\mu = \frac{E}{2(1 + v)}$$

where E is Young's modulus and for magnesium oxide was measured to be 2.51×10^{12} dynes per cm.^{2}

v is Poisson's ratio and assumed to be 0.35.

This gives $\mu = 9.3 \times 10^{11}$ dynes per cm.^{2}

b can be calculated from the lattice parameter.

This gives $b = 2.97 \times 10^{-8}$ cm.

Substitution of these values into the equation for the tension gives

$$T = 4.1 \times 10^{-4} \text{ dynes.}$$

The minimum shear stress[18] σ for dislocation glide at room temperature was measured to be $\sigma = 3.0 \times 10^{8}$ dynes per cm.^{2}

Using the equation $D = \frac{2T}{\sigma b}$ where D is the diameter of the smallest stable dislocation loop and T, σ and b, as defined above, gives upon substitution

$$D \approx 1 \text{ micron}$$

The actual value of D can differ from this value considerably. The calculated value is no more accurate than the equations and values used for this calculation.

APPENDIX VIII

Thermodynamic Calculations.

(a) Dissociation of nickel oxide.

$$2\ NiO \rightleftharpoons 2\ Ni + O_2$$

The nickel oxide will be just stable when the free energy change

$$\Delta F = 0$$

At 1 atm. pressure of O_2 at 1500°C

$$\Delta F = +32{,}000 \text{ cal. per gram mol. } O_2$$

At any other pressure

$$\Delta F = +32{,}000 + 4.575 \times 1773 \log P_{O_2}$$

$$= 0$$

therefore $$\log P_{O_2} = \frac{32{,}000}{4.575 \times 1773}$$

$$= -3.94$$

therefore $$P_{O_2} = 10^{-4} \text{ atm.}$$

$$= .76 \text{ mm. Hg.}$$

As the total pressure in the system is approximately 10^{-4} to 10^{-5} mm. Hg, the nickel oxide will completely dissociate. This is supported by the experimental observation that the nickel oxide coating which formed on the nickel drop, originally containing 2% nickel oxide, gradually disappeared.

(b) Dissociation of magnesium oxide

$$2\ MgO \rightleftharpoons 2\ Mg + O_2$$

The magnesium oxide will be just stable when the free energy change

$$\Delta F = 0$$

At 1 atm. O_2 and 1500°C

$$\Delta F = +184{,}000 \text{ cal. per gram mol. } O_2$$

at any other pressure

$$\Delta F = +184{,}000 + 4.575 \times 1773 \log P^2_{Mg}\, P_{O_2}$$

Letting $P_{Mg} = 2\, P_{O_2}$ gives

$$\log 4\, P^3_{O_2} = -22.7$$

or $$\log P^3_{O_2} = -23.3$$

$$P_{O_2} = 10^{-7.8} \text{ atm.}$$

therefore

$$P_{Mg} = 10^{-7.5} \text{ atm.}$$

The total pressure of the system as indicated by the ionization gauge is approximately 10^{-5} mm. Hg or 1.3×10^{-8} atm. The partial pressure of oxygen will be lower than this value. Also, one should consider that, in addition to pumping, oxygen is continuously removed by oxidation of the molybdenum. The oxygen partial pressure might therefore be substantially lower than the pressure calculated. In order to satisfy the equilibrium constant, the partial pressure of the magnesium must be increased. The magnesium oxide will therefore dissociate. This is supported by the observation that magnesium oxide gradually volatilizes at these temperatures and pressures.

(c) Calculation of thickness of interfacial layer of magnesium-nickel compound.

This calculation is based on a calculation by Williams and Murray[36] for the system Al_2O_3 - Cr in which it was shown that the formation of a solid solution at the interface results in a lowering of the surface tension.

By equating the free energy of formation of the compound to the energy required to lower the interfacial tension to zero, the thickness of the

interfacial layer can be calculated.

The free energy change during the formation of a solid solution or compound

$$\Delta F = \Delta H + RT(N_1 \ln N_1 + N_2 \ln N_2)$$

where ΔH is the heat of formation and

$-R(N_1 \ln N_1 + N_2 \ln N_2)$ is the entropy of mixing. R is the gas constant and N_1 and N_2 are the molar fractions of the compound.

ΔH may be assumed[37] to be approximately -2,000 calories per gram mole. The term $-R(N_1 \ln N_1 + N_2 \ln N_2)$ can be calculated to be 1.28. This gives

$$\Delta F = -2{,}000 - 1.28\ T$$

at 1500°C $\Delta F = -2{,}000 - 2{,}270$

$= -4{,}270$ calories per gram mole

$= -1.79 \times 10^{11}$ ergs per gram mole.

As the compound is located at the interface the change in free energy may be related to a decrease in the interfacial tension.

The relation between area and thickness is given by

$$\text{area} \times \text{thickness} = \text{molar volume}$$

$$= \frac{\text{mol. weight of compound}}{\text{density}}$$

The molecular weight can be calculated to be 107.3 grams per mol. The density can be calculated from the lattice parameters to be 3.47 grams per cc.

therefore area x thickness $= \frac{107.3}{3.47} = 30.9$

$\therefore$ free energy change per cc. $= -\frac{1.79 \times 10^{11}}{30.9}$

$= -5.79 \times 10^{9}$ ergs per cc.

The interfacial tension between nickel and magnesium oxide can be determined from the wettability data. The equation relating the interfacial

tension and the surface tensions is

$$\gamma_{MgO-Ni} = \gamma_{MgO} - \gamma_{Ni} \cos \theta$$

where γ_{MgO-Ni} is the interfacial tension

γ_{MgO} is the surface tension of the magnesium oxide and calculated[38] to be approximately 890 ergs/cm.^{2} at 1500°C.

γ_{Ni} is the surface tension of liquid nickel and was measured[11] to be 1845 ergs/cm.^{2}

Taking $\theta = 102°$ gives for the interfacial tension

$$\gamma_{MgO-Ni} = 890 + .2 \times 1845$$
$$= 1270 \text{ ergs/cm.}^2$$

For wetting to occur, θ must equal 0, i.e., cos θ equal 1. This limiting condition gives

$$\gamma_{MgO-Ni} = 890 - 1845$$
$$= -955 \text{ ergs/cm.}^2$$

Therefore the total decrease in interfacial tension which must take place, if wetting is to be achieved, is

$$-(1270 + 955) = -2225 \text{ ergs/cm.}^2$$

Equating the decrease in interfacial tension to the free energy change of formation gives an interfacial thickness of

$$\frac{2225}{5.79 \times 10^9} \text{ cm.}$$
$$= 38.4 \text{ Å}$$

Therefore, assuming that the parameters used in this calculation are correct, 38.4 Å is the minimum thickness of the interfacial layer if complete wetting

is to take place. The actual thickness of the interfacial layer exceeded this figure substantially as a much thicker layer for X-ray analysis was removed, which contained little or no nickel.

BIBLIOGRAPHY

1. White, A.E.S., Earp, E.K., Blakeley, T.H. and Walker, J., Symposium on Powder Metallurgy, 311 (1954).
2. Kingery, W.D., J. Am. Ceram. Soc., 36, 362 (1953).
3. Economos, G. and Kingery, W.D., J. Am. Ceram. Soc., 36, 403 (1953).
4. Himenik, M..Jr. and Kingery, W.D., J. Am. Ceram. Soc., 37, 18 (1954).
5. Kingery, W.D., J. Am. Ceram. Soc., 37, 42 (1954).
6. Johnston, P.D., J. Am. Ceram. Soc., 33, 168 (1950).
7. Allen, B.C. and Kingery, W.D., A.I.M.E. Trans., 215, 30 (1959).
8. Moore, D.G. and Thornton, H.P., J. Res. Nat. Bur. Standards, 62, 127 (1959).
9. Ellefson, B.S. and Taylor, N.W., J. Am. Ceram. Soc., 21, 193 (1938).
10. Ellefson, B.S. and Taylor, N.W., J. Am. Ceram. Soc., 21, 205 (1938).
11. Clarke, J.F., Thesis, Univ. of British Columbia, 1959.
12. King, B.W., Tripp, H.P. and Duckworth, W.H., Paper at 58th Meeting of Am. Ceram. Soc., New York City, 1956.
13. Cronin, L.J., Bull. Am. Ceram. Soc., 30, 234 (1951).
14. Norton Company, Customer Bulletin, CP 843.
15. Parker, E.R., Pask, J.A., Washburn, J., Gorum, A.E. and Luhmann, W., Journal of Metals, 10, 351 (1958)
16. Gorum, A.E., Parker, E.R. and Pask, J.A., J. Am. Ceram. Soc., 41, 161 (1958).
17. Washburn, J., Gorum, A.E. and Parker, E.R., A.I.M.E. Trans., 215, 230 (1959)
18. Stokes, R.J., Johnston, T.L. and Li, C.H., A.I.M.E. Trans., 215, 437 (1959).
19. Johnston, T.L., Stokes, R.J. and Li, C.H., Honeywell Research Center, Fourth Technical Report, (Feb. 1959).
20. Handbook of Chemistry and Physics, 36, 2062 (1956).
21. Kingery, W.D., J. Am. Ceram. Soc., 38, 3 (1955).
22. MacFarlane, W. Jr., Metallurgical Club Journal, 8, 15 (1955).

Bibliography (cont'd.)

23. Levin, E.M., McCurdie, H.F. and Hall, F.P., Phase Diagrams for Ceramists Am. Cer. Soc. Inc. (1956).

24. Brice, and Strong, Bull. Am. Phys. Soc., 9, 6 (1939).

25. Ditchborn, R.W., Nature, 136, 70 (1935).

26. Turnbull, R.C., Monthly Progress Report No. 214, Alfred University, Alfred, N.Y.

27. Pask, J.A., Private communication.

28. Gorum, A.E., Parker, E.R. and Pask, J.A., J. Am. Ceram. Soc., 41, 161 (1958)

29. Gilman, J.J., A.I.M.E. Trans., 212, 310 (1958).

30. Gorum, A.E., Private communication.

31. Jessop, H.T., and Harris, F.C., Photoelasticity. Cleaver-Hume Press,Ltd., London.

32. Kingery, W.D., J. Am. Ceram. Soc., 38, 3 (1955).

33. Handbook of Chemistry and Physics, 36th Ed. Chemical Rubber Publishing Co.

34. Metals Handbook, A.S.M. (1948).

35. Timoshenko, W. and Goodier, J.N., Theory of Elasticity, McGraw-Hill.

36. Williams, L.S. and Murray, P., Metallurgia 49, 210 (1954).

37. Samis, C.S., Private communication.

38. Livey, D.T. and Murray, P., J. Am. Ceram. Soc., 39, 363 (1956).

39. Gilman, J.J., A.I.M.E. Trans. 209, 449 (1957).

40. Cottrell, A.H., Dislocations and Plastic Flow in Crystals, Clarendon Press.

41. Winkler, H.G.F., Struktur und Eigenschaften der Kristalle, Springer Verlag (1955).